

Sparse Group Fused Lasso for Model Segmentation

A Hybrid Approach

David Degras

October 9, 2020

Abstract

This article introduces the sparse group fused lasso (SGFL) as a statistical framework for segmenting sparse regression models with multivariate time series. To compute solutions of the SGFL, a nonsmooth and nonseparable convex program, we develop a hybrid optimization method that is fast, requires no tuning parameter selection, and is guaranteed to converge to a global minimizer. In numerical experiments, the hybrid method compares favorably to state-of-the-art techniques with respect to computation time and numerical accuracy; benefits are particularly substantial in high dimension. The method's statistical performance is satisfactory in recovering nonzero regression coefficients and excellent in change point detection. An application to air quality data is presented. The hybrid method is implemented in the R package `sparseGFL` available on the author's Github page.

Keywords: Multivariate time series, model segmentation, high-dimensional regression, convex optimization, hybrid algorithm

1 Introduction

In the analysis of complex signals, using a single statistical model with a fixed set of parameters is rarely enough to track data variations over their entire range. In long and/or high-dimensional time series for example, the presence of nonstationarity, either in the form of slowly drifting dynamics or of abrupt regime changes, requires that statistical models flexibly account for temporal variations in signal characteristics. To overcome the intrinsic limitations of approaches based on a single model vis-à-vis heterogeneous and nonstationary signals, *model segmentation* techniques have been successfully employed in various fields including image processing (Alaíz et al. (2013); Friedman et al. (2007)) genetics (Bleakley and Vert (2011); Tibshirani and Wang (2007)), brain imaging Beer et al. (2019); Cao et al. (2018); Ombao et al. (2005); Xu and Lindquist (2015); Zhou et al. (2013), finance Hallac et al. (2019); Nystrup et al. (2017), industrial monitoring Saxén et al. (2016),

oceanography Ranalli et al. (2018), seismology Ohlsson et al. (2010), and ecology Alewijnse et al. (2018). Model segmentation consists in partitioning the domain of the signal (e.g. the temporal range of a time series or the lattice of a digital image) into a small number of segments or regions such that for each segment, the data are suitably represented with a single model. The models used to segment the data are typically of the same type (e.g. linear model) but differ by their parameters. The task of model segmentation is closely related to *change point detection* and is commonly referred to as (hybrid or time-varying) system identification in the engineering literature.

This work considers model segmentation in the following setup:

- *Structured multivariate data.* The observed data are multivariate predictor and response variables measured over a time grid.
- *Regression.* Predictor and response variables are related through a regression model, e.g. a linear model, generalized linear model, or vector autoregressive model.
- *High dimension.* There are far more predictors than response variables. However, at each measurement point, the responses only depend on a small number of predictors.

For simplicity, we present our methods and results in the context of linear regression, keeping in mind that our work readily extends to other regression models. Let $(X_t)_{1 \leq t \leq T}$ and $(y_t)_{1 \leq t \leq T}$ be multivariate time series where $y_t \in \mathbb{R}^d$ is a response vector and $X_t \in \mathbb{R}^{d \times p}$ a predictor matrix. We consider the time-varying multivariate linear model

$$y_t = X_t \beta_t + \varepsilon_t \tag{1}$$

where $\beta_t \in \mathbb{R}^p$ is an unknown regression vector and ε_t a random vector with mean zero. As noted above, we assume that $p \gg d$, that the β_t are sparse, and that $\beta_t = \beta_{t+1}$ for most values of t , that is, $\beta = (\beta_t)_{1 \leq t \leq T}$ is a piecewise constant function of t with few change points. Our goal is to develop efficient computational methods for estimating β and its change points $t : \beta_{t-1} \neq \beta_t$.

Before introducing the optimization problem at the core of this study, namely the *sparse group fused lasso* (SGFL), we review relevant work on model segmentation, change point detection, and structured sparse regression.

Related work

We first introduce some notations. Throughout the paper, $\|\cdot\|_q$ denotes the standard ℓ_q norm: $\|x\|_q = (\sum_{i=1}^n |x_i|^q)^{1/q}$ if $0 < q < \infty$ and $\|x\|_\infty = \max_{1 \leq i \leq n} (|x_i|)$ if $q = \infty$ for $x \in \mathbb{R}^n$. For convenience, we use the same notation $\beta = (\beta_1, \dots, \beta_T)$ to refer to regression coefficients either as a single vector in \mathbb{R}^{pT} or as a sequence of T vectors in \mathbb{R}^p .

Combinatorial approaches to change point detection. There is an extensive literature on change point detection spanning multiple fields and decades, which we only very partially describe here. For estimating changes in linear regression models, if the number $K \geq 2$ of segments (or equivalently the number $K - 1$ of change points) is fixed, the segmentation problem can be expressed as

$$\min_{\substack{(\beta_1, \dots, \beta_K) \in \mathbb{R}^{pK} \\ 1 < T_1 < \dots < T_{K-1} \leq T}} \frac{1}{2} \sum_{k=1}^K \sum_{t=T_{k-1}}^{T_k-1} \|y_t - X_t \beta_k\|_2^2 \quad (2)$$

with $T_0 = 1$ and $T_K = T + 1$. For a given set of change points (T_1, \dots, T_{K-1}) , the minimizing argument $\beta = (\beta_1, \dots, \beta_K)$ and associated objective value are obtained by ordinary least squares regression. Accordingly the optimization reduces to a combinatorial problem solvable by dynamic programming Bai and Perron (2003). This technique is computationally demanding as it requires performing $O(T^2)$ linear regressions before carrying out the dynamic program per se; the time spent in linear regression can however be reduced through recursive calculations. A fundamental instance of model segmentation in (2) occurs when the design matrix X_t is the identity matrix. In this case the problem is to approximate the signal (y_t) itself with a piecewise constant function.

If K is not prespecified, one may add a penalty function to (2) so as to strike a compromise between fitting the data and keeping the model complexity low. Examples of penalty functions on K include the Akaike Information Criterion (AIC), Bayesian Information Criterion (BIC), as well as more recent variants for high-dimensional data Chen and Chen (2008); Yao (1988). Another way to select K is to add/remove change points based on statistical tests or other criteria in top/down or bottom/up approaches. See Basseville and Nikiforov (1993) for a classical book on statistical change point detection and Truong et al. (2018) for a more recent survey. Readers interested in the popular method of binary segmentation may also consult Bai (1997); Fryzlewicz (2014); Leonardi and Bühlmann (2016).

Total variation penalty methods. Studying the piecewise constant approximation of 1-D signals, Friedman et al. (2007) utilize a convex relaxation of (2) called the *fused lasso signal approximation* (FLSA):

$$\min_{\beta \in \mathbb{R}^T} \frac{1}{2} \sum_{t=1}^T (y_t - \beta_t)^2 + \lambda_1 \sum_{t=1}^T |\beta_t| + \lambda_2 \sum_{t=1}^{T-1} |\beta_{t+1} - \beta_t|. \quad (3)$$

Here, hard constraints or penalties on the number K of segments are replaced by a penalty on the increments $\beta_{t+1} - \beta_t$. This total variation penalty promotes flatness in the profile of β , that is, a small number of change points. The ℓ_1 penalty on β , called a *lasso penalty* in the statistical literature, favors sparsity in β . The regularization parameters $\lambda_1, \lambda_2 > 0$

determine a balance between fidelity to the data, sparsity of β , and number of change points. They can be specified by the user or selected from the data, for example by cross-validation. Friedman et al. (2007) derive an efficient coordinate descent method to calculate the solution $\hat{\beta} = \hat{\beta}(\lambda_1, \lambda_2)$ to (3) along a path of values of (λ_1, λ_2) . Their method can also be applied to the more general problem of *fused lasso regression*

$$\min_{\beta \in \mathbb{R}^T} \frac{1}{2} \sum_{i=1}^n (y_i - x'_i \beta)^2 + \lambda_1 \sum_{t=1}^T |\beta_t| + \lambda_2 \sum_{t=1}^{T-1} |\beta_{t+1} - \beta_t| \quad (4)$$

where $x_i \in \mathbb{R}^T$ is a vector of predictors, although it is not guaranteed to yield a global minimizer in this case. One may recover the FLSA (3) by setting $n = T$ and taking the x_i as the canonical basis of \mathbb{R}^T in (4). More recent approaches to fused lasso regression include Hoeffding (2010); Liu et al. (2010); Wang et al. (2015a).

The FLSA and fused lasso can easily be adapted to the multivariate setup as follows:

$$\min_{\beta \in \mathbb{R}^{pT}} \frac{1}{2} \sum_{t=1}^T \|y_t - X_t \beta_t\|_2^2 + \lambda_1 \sum_{t=1}^T \|\beta_t\|_1 + \lambda_2 \sum_{t=1}^{T-1} \|\beta_{t+1} - \beta_t\|_1 \quad (5)$$

where $X_t \in \mathbb{R}^{d \times p}$, $y_t \in \mathbb{R}^d$, and $\beta = (\beta_1, \dots, \beta_T)$. These approaches are however not suitable for segmenting multivariate signals/models as they typically produce change points that are only shared by few predictor variables. This is because the ℓ_1 norm in the total variation penalty affects each of the p predictors separately. A simple way to induce change points common to all predictors is to replace this ℓ_1 norm by an ℓ_q norm with $q > 1$. Indeed for $q > 1$, the ℓ_q norm of \mathbb{R}^p is differentiable everywhere except at the origin, which promotes $\|\beta_{t+1} - \beta_t\|_q = 0$. Typically, for the model estimate to have a change point at time $t + 1$, a jump of at least modest size must occur in a significant fraction of the p time-varying regression coefficients between t and $t + 1$. Due to its computational simplicity, the ℓ_2 norm is often used in practice. For example, a common approach to denoising multivariate signals is to solve

$$\min_{\beta \in \mathbb{R}^{dT}} \frac{1}{2} \sum_{t=1}^T \|y_t - \beta_t\|_2^2 + \lambda_2 \sum_{t=1}^{T-1} w_t \|\beta_{t+1} - \beta_t\|_2 \quad (6)$$

where the w_t are positive weights. Bleakley and Vert (2011) reformulate this problem as a group lasso regression and apply the group LARS algorithm (see Yuan and Lin (2006)) to efficiently find solution paths $\hat{\beta} = \hat{\beta}(\lambda_2)$ as λ_2 varies. Wytock et al. (2014) propose Newton-type methods for (6) that extend to multichannel images. These two papers refer to problem (6) as the *group fused lasso* (GFL).

Related to (6) is the *convex clustering problem*

$$\min_{\beta \in \mathbb{R}^{pT}} \frac{1}{2} \sum_{t=1}^T \|y_t - \beta_t\|_2^2 + \lambda_2 \sum_{1 \leq s < t \leq T} w_{st} \|\beta_s - \beta_t\|_2 \quad (7)$$

where the β_t are cluster centroids (see Chi and Lange (2015); Hocking et al. (2011); Wang et al. (2018); Zhu et al. (2014) and the reference therein). This problem is arguably more difficult because there, the penalty pertains to all pairs of data points, as opposed to all pairs of successive data points. Also related to (6)-(7) is the problem of *penalized multinomial logistic regression* (Price et al. (2019)) where the squared loss function is replaced by the negative log-likelihood, $w_{st} = 1$, and the β_t represent regression vectors for T response categories. In this context the total variation penalty facilitates combining similar categories.

To segment multivariate regression models with group sparsity structure, Alaíz et al. (2013) consider a generalization of (6) that they also call group fused lasso:

$$\min_{\beta \in \mathbb{R}^{pT}} \frac{1}{2} \sum_{t=1}^T \|y_t - X_t \beta_t\|_2^2 + \lambda_1 \sum_{t=1}^T \|\beta_t\|_2 + \lambda_2 \sum_{t=1}^{T-1} w_t \|\beta_{t+1} - \beta_t\|_2. \quad (8)$$

They handle the optimization with a proximal splitting method similar to Dykstra’s projection algorithm. Songsiri (2015) studies (8) in the context of vector autoregressive models, using the well-known alternative direction method of multipliers (ADMM). See e.g. Combettes and Pesquet (2011) for an overview of proximal methods and ADMM.

Sparse Group Fused Lasso

Under our assumptions, the set of regression coefficients $\beta = (\beta_1, \dots, \beta_T)$ in the time-varying model $y_t = X_t \beta_t + \varepsilon_t$ is sparse and piecewise constant with few change points. To enforce these assumptions in fitting the model to data, we propose to solve

$$\min_{\beta \in \mathbb{R}^{pT}} F(\beta) := \frac{1}{2} \sum_{t=1}^T \|y_t - X_t \beta_t\|_2^2 + \lambda_1 \sum_{t=1}^T \|\beta_t\|_1 + \lambda_2 \sum_{t=1}^{T-1} w_t \|\beta_{t+1} - \beta_t\|_2. \quad (9)$$

Problem (9) has common elements with the fused lasso (5) and the group fused lasso (8) but the three problems are distinct and not reducible to one another. For example, (5) uses an ℓ_1 TV penalty that favors equality between successive regression vectors at the coordinate level, i.e. $(\beta_t)_k = (\beta_{t+1})_k$, whereas (9) uses an ℓ_2 TV penalty to promote blockwise equality $\beta_t = \beta_{t+1}$. This distinction is essential because the former tends to produce *local* change points, which may be difficult to interpret and unsuitable for model segmentation, whereas the latter promotes *global* change points at which most or all regression coordinates $(\beta_t)_k$ ($1 \leq k \leq p$) change value; see Bleakley and Vert (2011) for a numerical illustration. Also, unlike (8) which exploits an ℓ_2 penalty to induce group sparsity in β , (9) features a standard lasso penalty. To distinguish (9) from the group fused lasso problems (6)-(8), we call it *sparse group fused lasso* (SGFL). (Problem (9) is referred to as ℓ_2 variable fusion in Barbero and Sra (2011) but we have not found this terminology elsewhere in the literature.) The GFL (6) is a special case of (9) where $X_t = I_d$ (identity matrix) for all t and $\lambda_1 = 0$.

Remark 1 (Intercept). *A time-varying intercept vector δ_t can be added to the regression model, yielding $y_t = X_t\beta_t + \delta_t + \varepsilon_t$. While intercepts are typically not penalized in lasso regression, one must assume some sparsity in the increments $\delta_{t+1} - \delta_t$ for the extended model to be meaningful. Accordingly, the extended SGFL expresses as*

$$\begin{aligned} \min_{\beta, \delta} \frac{1}{2} \sum_{t=1}^T \|y_t - X_t\beta_t - \delta_t\|_2^2 + \lambda_1 \sum_{t=1}^T \|\beta_t\|_1 \\ + \lambda_2 \sum_{t=1}^{T-1} w_t \sqrt{\|\beta_{t+1} - \beta_t\|_2^2 + \|\delta_{t+1} - \delta_t\|_2^2}. \end{aligned} \tag{10}$$

For simplicity of exposition, we only consider problem (9) in this paper, noting that all methods and results easily extend to (10).

The objective function F in (9) has three components: a smooth function (squared loss), a nonsmooth but separable function (elastic net penalty), and a nonsmooth, nonseparable function (total variation penalty). We recall that a function $f(\beta_1, \dots, \beta_T)$ is said to be (block-)separable if it can be expressed as a sum of functions $\sum_{t=1}^T f_t(\beta_t)$. All three functions are convex. Accordingly, the SGFL (9) is a *nonsmooth, nonseparable convex program*. Several off-the-shelf methods can be found in the convex optimization literature for this type of problem, among which primal-dual algorithms take a preeminent place Condat (2013); Yan (2018). One could also utilize general-purpose convex optimization tools such as proximal methods (for instance, the Dykstra-like approach of Alaíz et al. (2013) can easily be adapted to (9)), ADMM and its variants, or even subgradient methods. However, these approaches do not take full advantage of the structure of (9), which may cause computational inefficiencies. In addition, these approaches aim at function minimization and not model segmentation or change point detection. As a result, they typically produce solutions for which every time t is a change point and where the task of recovering the “true” underlying change points (or segments) may be nontrivial. By devising customized methods for SGFL, one may expect substantial gains in computational speed while at the same time producing well-defined model segmentations.

Contributions and organization the paper

We make the following contributions with this paper.

1. We introduce the sparse group fused lasso (SGFL) for model segmentation in high dimension and develop a hybrid algorithm that efficiently solves the SGFL (Algorithm 5). The algorithm produces a sequence of solutions that monotonically decrease the objective function and converge to a global minimizer. It yields exact model segmentations, as opposed to general optimization methods that only provide approximate segmentations. Importantly, the hybrid algorithm does not require any complicated selection of tuning parameters from the user.
2. A key component of the hybrid algorithm is an iterative soft-thresholding scheme for computing the proximal operator of sums of ℓ_1 and ℓ_2 norms. This scheme, which is shown to converge linearly, is of independent interest and can serve as a building block in other optimization problems.
3. Regarding the implementation of the SGFL, we compare our hybrid approach to state-of-the-art optimization methods (e.g. ADMM, linearized ADMM, primal-dual) in terms of computational speed and numerical accuracy via numerical experiments. We also examine the statistical accuracy of the SGFL method, comparing it to recent methods for change point detection in high dimensional regression. In this second set of experiments, we pay particular attention to recovery of nonzero coefficients, change point detection, sparsity of the solution, and goodness of fit. We also illustrate the SGFL method with an application to air quality monitoring.
4. We implement the hybrid algorithm in the R package `sparseGFL` available at <https://github.com/ddegras/sparseGFL>.

The paper is organized as follows. Section 2 gives an overview of the hybrid algorithm. Section 3 details the calculations involved in each part of the algorithm. The full algorithm is summarized in Section 3.5 and its global convergence is stated. Section 4 presents numerical experiments comparing the proposed algorithm to state-of-the-art approaches both in terms of optimization performance and of statistical accuracy. An illustration of SGFL with air quality data is also given. Section 5 summarizes our results and outlines directions for future research. Appendix A contains a proof of linear convergence for the iterative soft-thresholding scheme used in the algorithm. Appendix B contains a proof of global convergence for the hybrid algorithm. Supplementary Materials include additional results related to the numerical experiments of Section 4.

2 Algorithm overview

Optimization strategy

The proposed algorithm operates at different levels across iterations or cycles. By increasing order of complexity and generality, the optimization of F in (9) may be conducted with respect to: 1) a single block β_t , 2) a chain of blocks $(\beta_t, \dots, \beta_{t+k})$ such that $\beta_t = \dots = \beta_{t+k}$ (*fusion chain*), 3) all fusion chains, 4) all blocks. The rationale for this hybrid optimization is to exploit problem structure for fast calculations while guaranteeing convergence to a global solution. By problem structure, we refer both to the block structure of the regression coefficients $\beta = (\beta_1, \dots, \beta_T)$ and to the piecewise nature of the regression model (1) over the time range $\{1, \dots, T\}$. The first two levels of optimization (single block and single chain) involve block coordinate descent methods that can be implemented very quickly in a serial or parallel fashion. Because the objective (9) is *not separable* in β_t , these methods do not guarantee convergence to a global solution. They only establish that the current solution $\hat{\beta}$ is *blockwise optimal* (Tseng (2001)), i.e. F cannot be further reduced by changing a single block or chain of fused blocks in $\hat{\beta}$. The next level (all fusion chains) involves an *active set* approach: assuming to have identified the optimal model segmentation, the associated fusion chains are fixed and F is minimized with respect to these chains. Denoting by K the number of chains, the dimension of the search space decreases from pT variables to pK where typically $K \ll T$. This third level of optimization is also not sufficient for global convergence. It ensures however that the minimum of F over the current model segmentation has been attained. The fourth level consists in a single iteration of the subgradient method, which is known to converge (albeit very slowly) to a global minimizer of F (e.g. (Bertsekas, 2015, Chap. 3)). Of the four optimization levels, this is the most general and most computationally intensive one. Once combined to form the proposed hybrid algorithm (Algorithm 5 in Section 3.5), these four optimization components guarantee convergence to a (global) minimizer of F (Theorem 2 in Section 3.5).

The general strategy of the hybrid algorithm is to optimize at the lowest (and fastest) level whenever possible. More precisely, optimization is realized at a higher level only when it is impossible to reduce the objective F at the current level or a lower level. The flow of these operations is outlined below.

- Step 1.** For each t , optimize the objective function F in (9) with respect to β_t while keeping all other blocks fixed to their current values. Cycle through blocks until F cannot be further reduced, then go to Step 2.
- Step 2.** Let $T_2 < \dots < T_K$ be the change points associated to the current solution $\hat{\beta}$ (if any) and $C_k = \{t : T_k \leq t < T_{k+1}\}$ the corresponding fusion chains ($1 \leq k \leq K$) with $T_1 = 1$ and $T_{K+1} = T + 1$. For each k , optimize F with respect to $(\beta_t)_{t \in C_k}$ under the constraint $\beta_{T_k} = \dots = \beta_{T_{k+1}-1}$ while keeping all blocks outside C_k fixed to their current values. Temporarily fuse C_k with C_{k+1} and repeat the optimization under the constraint $\beta_{T_k} = \dots = \beta_{T_{k+2}-1}$. If F has been reduced, update the blocks $(\beta_t)_{t \in C_k \cup C_{k+1}}$ to their common value and fuse C_k with C_{k+1} . Cycle through fusion chains until F cannot be further reduced. If F has been reduced at any point during Step 2, go back to Step 1. Otherwise, go to Step 3.
- Step 3.** Fix the current fusion chains and optimize F with respect to $(\beta_{T_1}, \dots, \beta_{T_K})$ under the constraints $\beta_{T_k} = \dots = \beta_{T_{k+1}-1}$ ($1 \leq k \leq K$). Go to Step 4.
- Step 4.** Check the optimality of the current solution $\hat{\beta}$ by calculating a subgradient $g \in \partial F(\hat{\beta})$ of minimal norm. If g is (approximately) zero, terminate the algorithm and output $\hat{\beta}$. Otherwise, take a subgradient step in the direction $-g$ and go back to Step 1.

We now give an overview of each of the four algorithm steps above.

2.1 Block coordinate descent

The principle of block coordinate descent is to partition the optimization variables into blocks and to optimize the objective function at each iteration with respect to a given block while keeping the other blocks fixed. In the optimization (9), time provides a natural blocking structure. Given a current solution $\hat{\beta} = (\hat{\beta}_1, \dots, \hat{\beta}_T)$ and a time index $t \in \{1, \dots, T\}$, the problem formulates as

$$\min_{\beta_t \in \mathbb{R}^p} F(\hat{\beta}_1, \dots, \hat{\beta}_{t-1}, \beta_t, \hat{\beta}_{t+1}, \dots, \hat{\beta}_T).$$

Eliminating terms in F that do not depend on β_t , this amounts to

$$\min_{\beta_t \in \mathbb{R}^p} \frac{1}{2} \|y_t - X_t \beta_t\|_2^2 + \lambda_1 \|\beta_t\|_1 + \lambda_2 \left(w_{t-1} \|\beta_t - \hat{\beta}_{t-1}\|_2 + w_t \|\hat{\beta}_{t+1} - \beta_t\|_2 \right). \quad (11)$$

To accommodate the cases $t = 1$ and $t = T$, we set $w_0 = w_T = 0$ and $\hat{\beta}_0 = \hat{\beta}_{T+1} = 0_p$.

Problem (11) cannot be solved in closed form. Instead, we solve it using the fast iterative soft-thresholding algorithm (FISTA) of Beck and Teboulle (2009), a proximal gradient method that enjoys the accelerated convergence rate $O(1/n^2)$, with n the number of iterations. This algorithm is described in Section 3.1. The application of FISTA to (11)

entails calculating the proximal operator of the sum of the lasso and total variation penalties. As a reminder, the proximal operator of a convex function $g : \mathbb{R}^p \rightarrow \mathbb{R}$ is defined by $\text{prox}_g(x) = \text{argmin}_{y \in \mathbb{R}^p} g(y) + (1/2)\|y - x\|_2^2$. Although the proximal operator of each penalty easily obtains in closed form, determining the proximal operator of their sum is highly nontrivial. For this purpose, we develop an iterative soft-thresholding algorithm described in Section 3.2.

The optimization (11) is repeated over a sequence of blocks and the solution $\hat{\beta}$ is updated each time until the objective function F in (9) cannot be further reduced. The order in which the blocks are selected for optimization is called the *sweep pattern*. Common examples of sweep patterns include cyclic (e.g. Tseng (2001)), cyclic permutation, (e.g. Nesterov (2012)), and greedy selection (e.g. Li and Osher (2009)). The block coordinate descent is summarized in Algorithm 1.

Algorithm 1 Block Coordinate Descent

Input: $\beta^{n-1} \in \mathbb{R}^{pT}$, sweeping pattern (t_1, \dots, t_T)

Output: $\beta^n \in \mathbb{R}^{pT}$

$\hat{\beta} \leftarrow \beta^{n-1}$

for $t = t_1, t_2, \dots, t_T$ **do**

 Check (17)-(18)-(19) for a simple solution to (11)

if simple solution **then**

$\hat{\beta}_t \leftarrow \hat{\beta}_{t-1}$ or $\hat{\beta}_t \leftarrow \hat{\beta}_{t+1}$ as required

else {FISTA}

 Set $f(\beta_t) = \frac{1}{2} \|y_t - X_t \beta_t\|_2^2$, $g(\beta_t) = \lambda_1 \|\beta_t\|_1 + \lambda_2 (w_{t-1} \|\beta_t - \hat{\beta}_{t-1}\|_2 + w_t \|\hat{\beta}_{t+1} - \beta_t\|_2)$

 Apply Algorithm 3 to $f + g$ with starting point $\hat{\beta}_t$, Lipschitz constant $L = \|X_t' X_t\|_2$, and $\text{prox}_{g/L}$ given by (23)-(24). Output β_t^+

$\hat{\beta}_t \leftarrow \beta_t^+$

end if

$\beta_t^n \leftarrow \hat{\beta}_t$

end for

2.2 Fusion cycle: single chain

Because the total variation penalty in F is nonsmooth and nonseparable, the block coordinate descent can get stuck in points that are blockwise optimal but not globally optimal; see Tseng (2001) for a theoretical justification and Friedman et al. (2007) for an example. To overcome this difficulty, one may constrain two or more consecutive blocks $\beta_t, \beta_{t+1}, \dots$ to be equal and optimize F with respect to their common value while keeping other blocks fixed. This fusion strategy is well suited to segmentation because it either preserves segments or merges them into larger ones. Given a current solution $\hat{\beta} = (\hat{\beta}_1, \dots, \hat{\beta}_T)$, the time

range $\{1, \dots, T\}$ is partitioned into segments or fusion chains $C_k = \{t : T_k \leq t < T_{k+1}\}$ ($1 \leq k \leq K$) such that the $\hat{\beta}_{T_k} = \dots = \hat{\beta}_{T_{k+1}-1}$ and that $\hat{\beta}_{T_k} \neq \hat{\beta}_{T_{k+1}}$. By convention we set $T_1 = 1$ and $T_{K+1} = T + 1$. If $K > 1$, T_2, \dots, T_K are the estimated change points of the regression model $y_t = X_t \beta_t + \varepsilon_t$. The algorithm successively optimizes (9) over each fusion chain C_k while enforcing the equality constraint $\beta_{T_k} = \dots = \beta_{T_{k+1}-1}$:

$$\min_{\beta_t \in \mathbb{R}^p} F(\hat{\beta}_1, \dots, \hat{\beta}_{T_k-1}, \beta_t, \dots, \beta_t, \hat{\beta}_{T_{k+1}}, \dots, \hat{\beta}_T)$$

where β_t is repeated $n_k = T_{k+1} - T_k$ times. This works out as

$$\begin{aligned} \min_{\beta_t \in \mathbb{R}^p} \left\{ \frac{1}{2} \sum_{s=T_k}^{T_{k+1}-1} \|y_s - X_s \beta_t\|_2^2 + \lambda_1 n_k \|\beta_t\|_1 \right. \\ \left. + \lambda_2 \left(w_{T_k-1} \|\beta_t - \hat{\beta}_{T_k-1}\|_2 + w_{T_{k+1}} \|\beta_t - \hat{\beta}_{T_{k+1}}\|_2 \right) \right\}. \end{aligned} \quad (12)$$

The algorithm may also try to merge two consecutive fusion chains to form a larger chain. To be precise, as t follows a given sweeping pattern t_1, \dots, t_T , the algorithm either: (i) solves (12) if $t = T_k$ and $T_{k+1} - T_k > 1$ (start of a non-singleton chain), (ii) solves (12) with each T_{k+1} replaced by T_{k+2} and n_k by $n_k + n_{k+1}$ if $t = T_{k+1} - 1$ and $t < T$ (end of a chain), or (iii) skips to the next value of t in other cases. The optimization (12) is performed in the same way as the block coordinate descent (11) (FISTA + iterative soft-thresholding). The fusion cycle for single chains is summarized in Algorithm 2.

2.3 Fusion cycle: all chains

When no further reduction can be achieved in F by changing a single block or single fusion chain in the current solution $\hat{\beta} \in \mathbb{R}^{pT}$, a logical next step is to optimize F with respect to *all* fusion chains. Specifically, one identifies the fusion chains $C_k = \{t : T_k \leq t < T_{k+1}\}$ ($1 \leq k \leq K$) over which $\hat{\beta} = (\hat{\beta}_t)$ is constant and optimizes F with respect to all blocks β_t under the equality constraints induced by the fusion chains:

$$\min_{\beta_{T_1}, \dots, \beta_{T_K} \in \mathbb{R}^p} F(\beta_{T_1}, \dots, \beta_{T_1}, \dots, \beta_{T_K}, \dots, \beta_{T_K})$$

with each β_{T_k} repeated $n_k = T_{k+1} - T_k$ times. Explicitly, this amounts to

$$\begin{aligned} \min_{\beta_{T_1}, \dots, \beta_{T_K}} \left\{ \frac{1}{2} \sum_{k=1}^K \sum_{t=T_k}^{T_{k+1}-1} \|y_t - X_t \beta_{T_k}\|_2^2 + \lambda_1 \sum_{k=1}^K n_k \|\beta_{T_k}\|_1 \right. \\ \left. + \lambda_2 \sum_{k=1}^{K-1} w_{T_{k+1}-1} \|\beta_{T_{k+1}} - \beta_{T_k}\|_2 \right\}. \end{aligned} \quad (13)$$

Algorithm 2 Fusion Cycle: Single Chain

Input: $\beta^{n-1} \in \mathbb{R}^{pT}$, sweeping pattern (t_1, \dots, t_T)

Output: β^n

$\hat{\beta} \leftarrow \hat{\beta}^{n-1}$

Determine fusion chains C_1, \dots, C_K and chain starts $T_1 \leq \dots \leq T_K$

for $t = t_1, t_2, \dots, t_T$ **do**

if $t = T_k$ for some k and $T_{k+1} - T_k > 1$ **then** {chain start}

$a \leftarrow T_k, \quad b \leftarrow T_{k+1} - 1$

else if $t = T_{k+1} - 1$ for some $k < K$ **then** {chain end}

$a \leftarrow T_k, \quad b \leftarrow T_{k+2} - 1$

else {chain interior}

 Skip to next t

end if

 Set $f(\beta_t) = \frac{1}{2} \sum_{s=a}^b \|y_s - X_s \beta_t\|_2^2$

 Set $g(\beta_t) = \lambda_1(b - a + 1) \|\beta_t\|_1 + \lambda_2(w_{a-1} \|\beta_t - \hat{\beta}_{a-1}\|_2 + w_b \|\hat{\beta}_{b+1} - \beta_t\|_2)$

 Check (26)-(27)-(28) for a simple solution to $\min(f + g)$

if simple solution **then**

$\beta_t^+ \leftarrow \hat{\beta}_{a-1}$ or $\beta_t^+ \leftarrow \hat{\beta}_{b+1}$ as required

else {FISTA}

 Apply Algorithm 3 to $f + g$ with starting point $\hat{\beta}_t$, Lipschitz constant $L = \|\sum_{s=a}^b X_s' X_s\|_2$, and $\text{prox}_{g/L}$ given by (29). Output β_t^+

end if

$\beta^+ \leftarrow (\hat{\beta}_1, \dots, \hat{\beta}_{a-1}, \beta_t^+, \dots, \beta_t^+, \hat{\beta}_{b+1}, \dots, \hat{\beta}_T) \in \mathbb{R}^{pT}$

if $b = T_{k+2} - 1$ and $F(\beta^+) < F(\hat{\beta})$ **then** {merge C_k and C_{k+1} }

 Remove T_{k+1} from $\{T_1, \dots, T_K\}$, set $K \leftarrow K - 1$, relabel chain starts as $T_1 \leq \dots \leq T_K$, and set $T_{K+1} \leftarrow T + 1$

end if

$\hat{\beta}_s \leftarrow \beta_t^+$ and $\beta_s^n \leftarrow \beta_t^+$ for $T_k \leq s < T_{k+1}$

end for

To solve (13) we employ a version of FISTA slightly different from the one used in (11) and (12). In particular this version (Algorithm 4) operates under the requirement that $\beta_{T_k} \neq \beta_{T_{k+1}}$ for all k . If two blocks β_{T_k} and $\beta_{T_{k+1}}$ become equal during the optimization, the corresponding fusion chains C_k and C_{k+1} are merged and problem (13) is restarted. Details are given in Section 3.3.

2.4 Checking the optimality of a solution

A vector $x \in \mathbb{R}^n$ ($n \geq 1$) minimizes a convex function $f : \mathbb{R}^n \rightarrow \mathbb{R}$ if and only if 0_n is a *subgradient* of f at x . (The concept of subgradient generalizes the gradient to possibly nondifferentiable convex functions.) This expresses equivalently as the membership of 0_n to the *subdifferential* $\partial f(x)$, that is, the set of all subgradients of f at x . Definition, basic properties, and examples of subgradients and subdifferentials can be found in textbooks on convex analysis, e.g. Rockafellar (2015).

In order to formulate the optimality conditions of the SGFL problem (9), we define the sign operator

$$\text{sgn}(x) = \begin{cases} \{1\} & \text{if } x > 0, \\ \{-1\} & \text{if } x < 0, \\ [-1, 1] & \text{if } x = 0, \end{cases}$$

for $x \in \mathbb{R}$ and extend it as a set-valued function from \mathbb{R}^n to \mathbb{R}^n in a componentwise fashion: $(\text{sgn}(x))_i = \text{sgn}(x_i)$ ($1 \leq i \leq n$). Now, a vector $\hat{\beta} = (\hat{\beta}_1, \dots, \hat{\beta}_T) \in \mathbb{R}^{pT}$ minimizes F if and only if 0_{pT} is a subgradient at $\hat{\beta}$, that is, if and only if there exist vectors $u_1, \dots, u_T \in \mathbb{R}^p$ and $v_1, \dots, v_{T-1} \in \mathbb{R}^p$ satisfying

$$X'_t(X_t \hat{\beta}_t - y_t) + \lambda_1 u_t + \lambda_2 (w_{t-1} v_{t-1} - w_t v_t) = 0_p \quad (14a)$$

and

$$u_t \in \text{sgn}(\hat{\beta}_t) \quad (14b)$$

for $1 \leq t \leq T$ as well as

$$\begin{cases} v_t = \frac{\hat{\beta}_{t+1} - \hat{\beta}_t}{\|\hat{\beta}_{t+1} - \hat{\beta}_t\|_2} & \text{if } \hat{\beta}_t \neq \hat{\beta}_{t+1}, \\ \|v_t\|_2 \leq 1 & \text{if } \hat{\beta}_t = \hat{\beta}_{t+1}, \end{cases} \quad (14c)$$

for $1 \leq t \leq T - 1$. By convention we take $v_0 = v_T = 0_p$. Conditions (14b)-(14c) arise from the facts that the subdifferential of the ℓ_1 norm is the sign operator and that the subdifferential of the ℓ_2 norm at 0_p is the ℓ_2 -unit ball of \mathbb{R}^p .

The optimality conditions (14a)-(14b)-(14c) can be checked by solving

$$\min_{U \in \mathcal{C}_1, V \in \mathcal{C}_2} \frac{1}{2} \|Z + \lambda_1 \alpha U + \lambda_2 V W D'\|_F^2 \quad (15)$$

where $U = (u_1, \dots, u_T) \in \mathbb{R}^{p \times T}$, $V = (v_1, \dots, v_{T-1}) \in \mathbb{R}^{p \times (T-1)}$, $Z = (z_1, \dots, z_T) \in \mathbb{R}^{p \times T}$ with $z_t = X_t'(X_t \hat{\beta}_t - y_t) + \lambda_1(1 - \alpha)\hat{\beta}_t$, and $D \in \mathbb{R}^{T \times (T-1)}$ is the differencing matrix given by $(D)_{ij} = -1$ if $i = j$, $(D)_{ij} = 1$ if $i = j + 1$, and $(D)_{ij} = 0$ otherwise. (Here we use matrix formalism to express (14a) more simply.) The sets \mathcal{C}_1 and \mathcal{C}_2 embody the constraints (14b) and (14c), respectively. If the minimum of (15) is zero, then 0_{pT} is a subgradient of F at $\hat{\beta}$ and $\hat{\beta}$ minimizes F . In this case the optimization is over.

A closer examination of (14a)-(14b)-(14c) reveals that change points in $\hat{\beta}$ break the global problem (15) into independent subproblems. More precisely, let $T_2 < \dots < T_K$ be the change points induced by $\hat{\beta}$ (assuming there is at least one) and C_1, \dots, C_K the associated segmentation of $\{1, \dots, T\}$. The constraints (14c) entirely determine the vectors v_{T_k-1} ($k \geq 2$), which breaks the coupling of the v_t separated by change points in (14a). On the other hand the constraints (14b) clearly affect each block u_t separately. Therefore, problem (15) can be solved separately (and in parallel) on each fusion chain C_k . We tackle (15) on each C_k using *gradient projection*. We embed this method inside FISTA for faster convergence. The necessary gradient calculation and projections on \mathcal{C}_1 and \mathcal{C}_2 are described in Section 3.4.

2.5 Subgradient step

If the attained minimum in (15) is greater than zero, then $\hat{\beta}$ is not a minimizer of F . By design of the hybrid algorithm, this implies that the segmentation C_1, \dots, C_K associated with $\hat{\beta}$ is suboptimal and that, starting from $\hat{\beta}$, F cannot be further reduced at the first three levels of optimization. In this case, arguments (U^*, V^*) that minimize (15) provide a subgradient $G = Z + \lambda_1 \alpha U^* + \lambda_2 V^* W D'$ of minimum norm. Denoting the vectorized version of G by $g \in \mathbb{R}^{pT}$, the opposite of g is a direction of steepest descent for F at $\hat{\beta}$ (e.g. Shor (1985)). Accordingly, at the fourth level of optimization, the algorithm takes a step in the direction $-g$ with step length obtained by exact line search. The updated solution expresses as $\beta^+ = \hat{\beta} - \alpha^* g$ where $\alpha^* = \operatorname{argmin}_{\alpha > 0} F(\hat{\beta} - \alpha g)$. The subgradient step accomplishes two important things: first, it moves the optimization away from the suboptimal segmentation C_1, \dots, C_K and second, by reducing the objective, it ensures that this segmentation will not be visited again later in the optimization. These properties and their consequence, namely the global convergence of the hybrid algorithm will be established in Theorem 2 in Section 3.5.

3 Algorithm details

This section gives a detailed account of how optimization is carried out at each level (single block, single fusion chain, all fusion chains, all blocks) in the main Algorithm 5. We first present the fast iterative soft-thresholding algorithm (FISTA) of Beck and Teboulle (2009) which we extensively use in Algorithm 5.

3.1 FISTA

Beck and Teboulle Beck and Teboulle (2009) consider the convex program

$$\min_{x \in \mathbb{R}^n} \{f(x) + g(x)\}$$

where $f : \mathbb{R}^n \rightarrow \mathbb{R}$ is a smooth convex function and $g : \mathbb{R}^n \rightarrow \mathbb{R}$ is a continuous convex function, possibly nonsmooth. Regarding the proposed hybrid algorithm for SGFL (Algorithm 5), the specific functions f, g used in applying FISTA are given in Algorithm 1 for block-level optimization, Algorithm 2 for optimization over a single chain, section 3.3 for optimization over all chains, and section 3.4 for verification of optimality.

The function f is assumed to be differentiable with Lipschitz-continuous gradient:

$$\|\nabla f(x) - \nabla f(y)\|_2 \leq L \|x - y\|_2$$

for all $x, y \in \mathbb{R}^n$ and some finite Lipschitz constant $L > 0$. The function g is assumed to be proximable, that is, its proximal operator $\text{prox}_{\gamma g}(x) = \arg \min_{y \in \mathbb{R}^n} \{g(y) + 1/(2\gamma)\|y - x\|_2^2\}$ should be easy to calculate for all $\gamma > 0$.

Their Iterative Soft Thresholding Algorithm (ISTA) is an iterative method that replaces at each iteration the difficult optimization of the objective $f + g$ by the simpler optimization of a quadratic approximation Q_L . Given a suitable vector $y \in \mathbb{R}^n$, the goal is to minimize

$$Q_L(x, y) = f(y) + \nabla f(y)'(x - y) + g(x) + \frac{L}{2} \|x - y\|_2^2. \quad (16)$$

with respect to $x \in \mathbb{R}^n$. With a few algebraic manipulations and omitting irrelevant additive constants, Q_L can be rewritten as

$$Q_L(x, y) = g(x) + \frac{L}{2} \left\| x - \left(y - \frac{1}{L} \nabla f(y) \right) \right\|_2^2$$

so that $\arg \min_x Q(x, y) = \text{prox}_{g/L}(y - (1/L)\nabla f(y))$. In other words, the minimization of Q_L is achieved through a gradient step with respect to f followed by a proximal step with respect to g . ISTA can thus be viewed as a proximal gradient method, also known as forward-backward method (e.g. Combettes and Pesquet (2011)). Observing that $Q_L(\cdot, y)$ majorizes $f + g$, ISTA can also be viewed as a majorization-minimization method. Formally, an iteration of ISTA expresses as $x^{n+1} = \arg \min_x Q_L(x, x^n) = \text{prox}_{g/L}(x^n - (1/L)\nabla f(x^n))$.

Proximal gradient methods are not new: they have been used for decades. The innovation of Beck and Teboulle (2009) is to accelerate the convergence of ISTA by introducing an auxiliary sequence (y^k) such that y^k is a well-chosen linear combination of x^{k-1} and x^k , the main solution iterates (see also Becker et al. (2011); Nesterov (2005) for related work). With this technique, the convergence rate of proximal gradient improves from $O(1/k)$ to

$O(1/k^2)$. Algorithm 3 presents this accelerated method, called Fast Iterative Soft Thresholding Algorithm (FISTA), in the case where a Lipschitz constant L is prespecified and kept constant through iterations. Algorithm 4 presents FISTA in the case where L is difficult to determine ahead of time and is chosen by backtracking at each iteration. This version of FISTA requires an initial guess L^0 for the Lipschitz constant as well as a factor $\eta > 1$ by which to increase the candidate value L in backtracking steps.

Algorithm 3 FISTA with constant step size

Input: $x^0 \in \mathbb{R}^n$, Lipschitz constant $L > 0$

Output: x^k

$$y^1 \leftarrow x^0, \alpha_1 \leftarrow 1$$

for $k = 1, 2, \dots$ **do**

$$x^k \leftarrow \text{prox}_{g/L} \left(y^k - \frac{1}{L} \nabla f(y^k) \right)$$

$$\alpha_{k+1} \leftarrow \frac{1 + \sqrt{1 + 4(\alpha_k)^2}}{2}$$

$$y^{k+1} \leftarrow x^k + \left(\frac{\alpha_k - 1}{\alpha_{k+1}} \right) (x^k - x^{k-1})$$

end for

Algorithm 4 FISTA with backtracking

Input: $x^0 \in \mathbb{R}^n$, $L^0 > 0$, $\eta > 1$

Output: x^k

$$y^1 \leftarrow x^0, \alpha_1 \leftarrow 1$$

for $k = 1, 2, \dots$ **do**

$$i \leftarrow 0$$

repeat

$$L \leftarrow \eta^i L^{k-1}$$

$$x^k \leftarrow \text{prox}_{g/L} \left(y^k - (1/L) \nabla f(y^k) \right)$$

$$i \leftarrow i + 1$$

until $(f + g)(x^k) \leq Q_L(x^k, y^k)$

$$L^k \leftarrow L$$

$$\alpha_{k+1} \leftarrow \frac{1 + \sqrt{1 + 4(\alpha_k)^2}}{2}$$

$$y^{k+1} \leftarrow x^k + \left(\frac{\alpha_k - 1}{\alpha_{k+1}} \right) (x^k - x^{k-1})$$

end for

3.2 Iterative soft-thresholding

In this section we present a novel iterative soft-thresholding algorithm for computing the proximal operators required in the application of FISTA to problems (11) and (12). We first examine the case of (11) (block coordinate descent) and then show how to adapt the

algorithm to (12) (optimization of F with respect to a single fusion chain). Of crucial importance is the soft-thresholding operator

$$S(x, \lambda) = \begin{cases} x + \lambda, & \text{if } x < -\lambda, \\ 0, & \text{if } |x| \leq \lambda, \\ x - \lambda, & \text{if } x > \lambda, \end{cases}$$

where $x \in \mathbb{R}$ and $\lambda \geq 0$ is a threshold. This operator accommodates vector arguments $x \in \mathbb{R}^p$ in a componentwise fashion: $(S(x, \lambda))_i = S(x_i, \lambda)$ ($1 \leq i \leq p$).

Checking for simple solutions. It is advantageous to verify whether $\hat{\beta}_{t-1}$ or $\hat{\beta}_{t+1}$ solves (11) before applying FISTA, which is more computationally demanding. The optimality conditions for (11) are very similar to those for the global problem (9), namely (14a)-(14b)-(14c), although of course the conditions for (11) pertain to a single time t . Hereafter we state these conditions in an easily computable form. Let $\phi : \mathbb{R}^p \times \mathbb{R}^p \times \mathbb{R}_+ \rightarrow \mathbb{R}^p$ be defined in a componentwise fashion by

$$(\phi(x, s, \lambda))_i = \begin{cases} x_i + \lambda_i & \text{if } s_i > 0, \\ x_i - \lambda_i & \text{if } s_i < 0, \\ S(x_i, \lambda_i) & \text{if } s_i = 0. \end{cases}$$

If $\hat{\beta}_{t-1} = \hat{\beta}_{t+1}$, this vector solves (11) if and only if

$$\left\| \phi(X_t'(X_t \hat{\beta}_{t-1} - y_t), \hat{\beta}_{t-1}, \lambda_1) \right\|_2 \leq \lambda_2(w_{t-1} + w_t). \quad (17)$$

If $\hat{\beta}_{t-1} \neq \hat{\beta}_{t+1}$, $\hat{\beta}_{t-1}$ solves (11) if and only if

$$\left\| \phi \left(X_t'(X_t \hat{\beta}_{t-1} - y_t) + \lambda_2 w_t \frac{\hat{\beta}_{t-1} - \hat{\beta}_{t+1}}{\|\hat{\beta}_{t-1} - \hat{\beta}_{t+1}\|_2}, \hat{\beta}_{t-1}, \lambda_1 \right) \right\|_2 \leq \lambda_2 w_{t-1} \quad (18)$$

and $\hat{\beta}_{t+1}$ solves (11) if and only if

$$\left\| \phi \left(X_t'(X_t \hat{\beta}_{t+1} - y_t) + \lambda_2 w_{t-1} \frac{\hat{\beta}_{t+1} - \hat{\beta}_{t-1}}{\|\hat{\beta}_{t+1} - \hat{\beta}_{t-1}\|_2}, \hat{\beta}_{t+1}, \lambda_1 \right) \right\|_2 \leq \lambda_2 w_t. \quad (19)$$

Fixed point iteration. After verifying that neither $\hat{\beta}_{t-1}$ nor $\hat{\beta}_{t+1}$ is a solution of (11), we apply Algorithm 3 (FISTA with constant step size) to (11) using the decomposition

$$\begin{cases} f(\beta_t) = \frac{1}{2} \|y_t - X_t \beta_t\|_2^2, \\ g(\beta_t) = \lambda_1 \|\beta_t\|_1 + \lambda_2 (w_{t-1} \|\beta_t - \hat{\beta}_{t-1}\|_2 + w_t \|\beta_t - \hat{\beta}_{t+1}\|_2). \end{cases} \quad (20)$$

The gradient of the smooth component f is $\nabla f(\beta_t) = X_t'(X_t\beta_t - y_t)$ with Lipschitz constant $L_t = \|X_t'X_t\|_2$. The main task is to calculate the proximal operator of g . Given a vector $z_t \in \mathbb{R}^p$, we seek

$$\text{prox}_{g/L_t}(z_t) = \underset{\beta_t \in \mathbb{R}^p}{\text{argmin}} g(\beta_t) + \frac{L_t}{2} \|\beta_t - z_t\|_2^2. \quad (21)$$

The optimality conditions for this problem are

$$0_p \in L_t(\beta_t - z_t) + \lambda_1 \text{sgn}(\beta_t) + \frac{\lambda_2 w_{t-1}}{\|\beta_t - \hat{\beta}_{t-1}\|_2}(\beta_t - \hat{\beta}_{t-1}) + \frac{\lambda_2 w_t}{\|\beta_t - \hat{\beta}_{t+1}\|_2}(\beta_t - \hat{\beta}_{t+1}) \quad (22)$$

or equivalently

$$\begin{aligned} & \left(L_t + \frac{\lambda_2 w_{t-1}}{\|\beta_t - \hat{\beta}_{t-1}\|_2} + \frac{\lambda_2 w_t}{\|\beta_t - \hat{\beta}_{t+1}\|_2} \right) \beta_t \\ & \in \left(L_t z_t + \frac{\lambda_2 w_{t-1} \hat{\beta}_{t-1}}{\|\beta_t - \hat{\beta}_{t-1}\|_2} + \frac{\lambda_2 w_t \hat{\beta}_{t+1}}{\|\beta_t - \hat{\beta}_{t+1}\|_2} \right) - \lambda_1 \alpha \text{sgn}(\beta_t). \end{aligned}$$

Given $\hat{\beta}_{t-1}$, $\hat{\beta}_{t+1}$ and z_t , we define the operator

$$\mathcal{T}(\beta_t) = \frac{S \left(L_t z_t + \frac{\lambda_2 w_{t-1} \hat{\beta}_{t-1}}{\|\beta_t - \hat{\beta}_{t-1}\|_2} + \frac{\lambda_2 w_t \hat{\beta}_{t+1}}{\|\beta_t - \hat{\beta}_{t+1}\|_2}, \lambda_1 \right)}{L_t + \frac{\lambda_2 w_{t-1}}{\|\beta_t - \hat{\beta}_{t-1}\|_2} + \frac{\lambda_2 w_t}{\|\beta_t - \hat{\beta}_{t+1}\|_2}} \quad (23)$$

for $\beta_t \in \mathbb{R}^p \setminus \{\hat{\beta}_{t-1}, \hat{\beta}_{t+1}\}$ and extend it by continuity: $\mathcal{T}(\hat{\beta}_{t-1}) = \hat{\beta}_{t-1}$ and $\mathcal{T}(\hat{\beta}_{t+1}) = \hat{\beta}_{t+1}$. The optimality conditions (22) now express as the fixed point equation

$$\mathcal{T}(\beta_t) = \beta_t.$$

The operator \mathcal{T} admits the fixed points $\hat{\beta}_{t-1}$, $\hat{\beta}_{t+1}$, and $\text{prox}_{g/L_t}(z_t)$. It can be shown that if $\text{prox}_{g/L_t}(z_t) \notin \{\hat{\beta}_{t-1}, \hat{\beta}_{t+1}\}$, the fixed points $\hat{\beta}_{t-1}$ and $\hat{\beta}_{t+1}$ are *repulsive* in the sense that there exist $\eta, \epsilon > 0$ such that $\|\mathcal{T}(\beta_t) - \hat{\beta}_{t-1}\|_2 \geq (1 + \epsilon)\|\beta_t - \hat{\beta}_{t-1}\|_2$ for $\|\beta_t - \hat{\beta}_{t-1}\|_2 \leq \eta$ (same for $\hat{\beta}_{t+1}$). This suggests calculating $\text{prox}_{g/L_t}(z_t)$ with the iterative soft-thresholding

$$\beta_t^{n+1} = \mathcal{T}(\beta_t^n). \quad (24)$$

Remark 2 (proximal gradient). *The fixed point iteration (23)-(24) can be viewed as a proximal gradient algorithm. Writing $g_1(\beta_t) = \lambda_1 \|\beta_t\|_1$ and $g_2(\beta_t) = \lambda_2 w_{t-1} \|\beta_t - \hat{\beta}_{t-1}\|_2 + \lambda_2 w_t \|\beta_t - \hat{\beta}_{t+1}\|_2 + (L_t/2) \|\beta_t - z_t\|_2^2$, it holds that*

$$\mathcal{T}(\beta_t) = \text{prox}_{\gamma g_1}(\beta_t - \gamma \nabla g_2(\beta_t)) \quad \text{with} \quad \frac{1}{\gamma} = L_t + \frac{\lambda_2 w_{t-1}}{\|\beta_t - \hat{\beta}_{t-1}\|_2} + \frac{\lambda_2 w_t}{\|\beta_t - \hat{\beta}_{t+1}\|_2}. \quad (25)$$

Remark 3 (Weiszfeld’s algorithm). *The fixed point iteration (23)-(24) is related in spirit to Weiszfeld’s algorithm Weiszfeld and Plastria (2009) and its generalizations (e.g. Kuhn (1973)) for the Fermat-Weber location problem $\arg \min_{y \in \mathbb{R}^p} \sum_{i=1}^m w_i \|y - x_i\|_2$, where $x_1, \dots, x_m \in \mathbb{R}^p$ and $w_1, \dots, w_m > 0$ are weights. Weiszfeld’s algorithm, in its generalized version, has iterates of the form*

$$y^{n+1} = \left(\sum_{i=1}^m \frac{w_i x_i}{\|y^n - x_i\|_2} \right) / \left(\sum_{i=1}^m \frac{w_i}{\|y^n - x_i\|_2} \right)$$

and is derived along the same lines as (23)-(24), namely by equating the gradient to zero and turning this equation into a fixed point equation.

By exploiting a connection to proximal gradient methods (2) and adapting the results of Bredies and Lorenz (2008) to a nonsmooth setting, we can establish the linear convergence of (23)-(24). We defer the proof of this result to Section A. For convenience, let us denote the proximal operator $\text{prox}_{g/L_t}(z_t)$ by β_t^* and the associated objective function by $\bar{g}(\beta_t) = g(\beta_t) + (L_t/2) \|\beta_t - z_t\|_2^2$. We also define the distance $r_n = \bar{g}(\beta_t^n) - \bar{g}(\beta_t^*)$ to the minimum of \bar{g} .

Theorem 1. *Assume that $\hat{\beta}_{t-1}$ and $\hat{\beta}_{t+1}$ are not solutions of (11), that $\beta_t^* \notin \{\hat{\beta}_{t-1}, \hat{\beta}_{t+1}\}$, and that the sequence $(\beta_t^n)_{n \geq 0}$ generated by (23)-(24) has its first term satisfying $\bar{g}(\beta_t^0) < \min(\bar{g}(\hat{\beta}_{t-1}), \bar{g}(\hat{\beta}_{t+1}))$. Then the distance $(r_n)_{n \geq 0}$ vanishes exponentially and $(\beta_t^n)_{n \geq 0}$ converges linearly to β_t^* , that is, there exist constants $C > 0$ and $\lambda \in [0, 1)$ such that*

$$\|\beta_t^n - \beta_t^*\|_2 \leq C\lambda^n.$$

The first two assumptions of Theorem 1 ensure that use of the iterative soft-thresholding (23)-(24) is warranted, in other words, that (11) and (21) do not have simple solutions. The condition on the starting point β_t^0 guarantees that the sequence (β_t^n) does not get stuck in $\hat{\beta}_{t-1}$ or $\hat{\beta}_{t+1}$. It is standard for this type of problem, see e.g. Kuhn (1973). In practice this condition is virtually always met by taking the current FISTA iterate as starting point.

Extension to fusion chains. When considering problem (12) over a fusion chain $C = \{t : a \leq t \leq b\}$, the objective decomposes as

$$\begin{cases} f(\beta_t) = \frac{1}{2} \sum_{s=a}^b \|y_s - X_s \beta_t\|_2^2, \\ g(\beta_t) = \lambda_1 n_C \|\beta_t\|_1 + \lambda_2 \left(w_{a-1} \|\beta_t - \hat{\beta}_{a-1}\|_2 + w_b \|\beta_t - \hat{\beta}_{b+1}\|_2 \right), \end{cases}$$

where $n_C = b - a + 1$. The conditions for $\hat{\beta}_{a-1}$ or $\hat{\beta}_{b+1}$ to be simple solutions of (12) are as follows. If $\hat{\beta}_{a-1} = \hat{\beta}_{b+1}$, this vector solves (12) if and only if

$$\left\| \phi \left(\sum_{s=a}^b X'_s (X_s \hat{\beta}_{a-1} - y_s), \hat{\beta}_{a-1}, \lambda_1 \right) \right\|_2 \leq \lambda_2 (w_{a-1} + w_b). \quad (26)$$

If $\hat{\beta}_{a-1} \neq \hat{\beta}_{b+1}$, $\hat{\beta}_{a-1}$ solves (12) if and only if

$$\left\| \phi \left(\sum_{s=a}^b X'_s (X_s \hat{\beta}_{a-1} - y_s) + \lambda_2 w_b \frac{\hat{\beta}_{a-1} - \hat{\beta}_{b+1}}{\|\hat{\beta}_{a-1} - \hat{\beta}_{b+1}\|_2}, \hat{\beta}_{a-1}, \lambda_1 \right) \right\|_2 \leq \lambda_2 w_{a-1} \quad (27)$$

and $\hat{\beta}_{b+1}$ solves (12) if and only if

$$\left\| \phi \left(\sum_{s=a}^b X'_s (X_s \hat{\beta}_{b+1} - y_s) + \lambda_2 w_{a-1} \frac{\hat{\beta}_{b+1} - \hat{\beta}_{a-1}}{\|\hat{\beta}_{b+1} - \hat{\beta}_{a-1}\|_2}, \hat{\beta}_{b+1}, \lambda_1 \right) \right\|_2 \leq \lambda_2 w_b. \quad (28)$$

If there are no simple solutions to (12), we apply Algorithm 3 to $f + g$. The gradient step is given by $\nabla f(\beta_t) = \sum_{s=a}^b X'_s (X_s \beta_t - y_s)$ and its Lipschitz constant $L_C = \|\sum_{s=a}^b X'_s X_s\|_2$. For a given $z_t \in \mathbb{R}^p$, the proximal operator $\text{prox}_{g/L_C}(z_t)$ is calculated by iteratively applying the soft-thresholding operator

$$\mathcal{T}_C(\beta_t) = \frac{S \left(L_C z_t + \frac{\lambda_2 w_{a-1} \hat{\beta}_{a-1}}{\|\beta_t - \hat{\beta}_{a-1}\|_2} + \frac{\lambda_2 w_b \hat{\beta}_{b+1}}{\|\beta_t - \hat{\beta}_{b+1}\|_2}, \lambda_1 n_C \right)}{L_C + \frac{\lambda_2 w_{a-1}}{\|\beta_t - \hat{\beta}_{a-1}\|_2} + \frac{\lambda_2 w_b}{\|\beta_t - \hat{\beta}_{b+1}\|_2}}. \quad (29)$$

3.3 Optimization over all fusion chains

The optimization (13) is carried out by applying Algorithm 4 (FISTA with backtracking) to $\min_{\beta \in \mathbb{R}^{pK}} (f + g)(\beta)$ where

$$\begin{cases} f(\beta) = \frac{1}{2} \sum_{k=1}^K \sum_{t=T_k}^{T_{k+1}-1} \|y_t - X_t \beta_k\|_2^2 + \lambda_2 \sum_{k=1}^{K-1} w_{T_{k+1}-1} \|\beta_{k+1} - \beta_k\|_2, \\ g(\beta) = \lambda_1 \sum_{k=1}^K n_k \|\beta_k\|_1. \end{cases}$$

For notational convenience, we have relabeled the vectors $\beta_{T_1}, \dots, \beta_{T_K}$ of (13) as β_1, \dots, β_K . Observe that f is nondifferentiable at points $\beta = (\beta_1, \dots, \beta_K)$ such that $\beta_k = \beta_{k+1}$ for some k , which violates the smoothness requirements of Section 3.1. We can nonetheless apply

FISTA until the algorithm either converges to a minimizer of $f + g$ or to a point of nondifferentiability for f . In the latter case, we merge the fusion chains C_k and C_{k+1} associated with the equality $\beta_k = \beta_{k+1}$ and restart FISTA with the reduced set of chains.

To fully specify the FISTA implementation, it remains to characterize the gradient of f and proximal operator of g . The former, wherever it exists, is given by ($1 \leq k \leq K$)

$$\begin{aligned} \frac{\partial f}{\partial \beta_k}(\beta) = & \sum_{t=T_k}^{T_{k+1}-1} X'_t(X_t \beta_k - y_t) + \lambda_2 w_{T_k-1} \frac{\beta_k - \beta_{k-1}}{\|\beta_k - \beta_{k-1}\|_2} \\ & + \lambda_2 w_{T_{k+1}-1} \frac{\beta_k - \beta_{k+1}}{\|\beta_k - \beta_{k+1}\|_2}. \end{aligned} \quad (30)$$

The proximal operator of g performs soft-thresholding by block ($1 \leq k \leq K$):

$$(\text{prox}_{g/L}(\beta))_k = S(\beta_k, \lambda_1 n_k). \quad (31)$$

3.4 Gradient projection method

Here we describe the method of Section 2.4 to check the optimality of a solution $\hat{\beta}$. For simplicity, we move the regularization parameters λ_1, λ_2 and diagonal weight matrix W from the objective in (15) to the constraint sets \mathcal{C}_1 and \mathcal{C}_2 . This is done with a simple change of variables.

Gradient step. Writing the objective as $f(U, V) = \frac{1}{2} \|Z + U + VD'\|_F^2$, the gradient of f is given by

$$\frac{\partial f}{\partial U}(U, V) = U + VD' + Z, \quad \frac{\partial f}{\partial V}(U, V) = UD + VD'D + ZD. \quad (32)$$

Therefore a Lipschitz constant L of $\nabla f(U, V)$ can be found by evaluating the spectral norm of the $(2T - 1) \times (2T - 1)$ matrix

$$\begin{pmatrix} I_T & D \\ D' & D'D \end{pmatrix}.$$

Standard calculations show that this matrix has spectral norm $1 + \|D'D\|_2$ and that the eigenvalues of $D'D$ are $\{2(1 - \cos(\frac{(2t-1)\pi}{2T})), 1 \leq t \leq T\}$. Combining these results, one can take $L = 5$.

Projection step. The orthogonal projection $P_{\mathcal{C}_1}(U)$ of $U \in \mathbb{R}^{p \times T}$ on \mathcal{C}_1 is obtained by applying fixed coefficient constraints and clamping values to the interval $[-\lambda_1, \lambda_1]$ where

needed. Its coefficients ($1 \leq t \leq T$, $1 \leq i \leq p$) are given by

$$(P_{\mathcal{C}_1}(U))_{it} = \begin{cases} \lambda_1 & \text{if } (\hat{\beta}_t)_i > 0, \\ -\lambda_1 & \text{if } (\hat{\beta}_t)_i < 0, \\ \min(\max((u_t)_i, -\lambda_1), \lambda_1) & \text{if } (\hat{\beta}_t)_i = 0. \end{cases} \quad (33)$$

The orthogonal projection $P_{\mathcal{C}_2}(V)$ of $V \in \mathbb{R}^{p \times (T-1)}$ on \mathcal{C}_2 is obtained by rescaling the columns of V ($1 \leq t < T$) as necessary:

$$(P_{\mathcal{C}_2}(V))_t = \min\left(\frac{\lambda_2 w_t}{\|v_t\|_2}, 1\right) v_t. \quad (34)$$

Writing $I_{\mathcal{C}}$ for the indicator function of a set \mathcal{C} ($I_{\mathcal{C}}(x) = 0$ if $x \in \mathcal{C}$ and $I_{\mathcal{C}}(x) = +\infty$ otherwise) and $g(U, V) = I_{\mathcal{C}_1}(U) + I_{\mathcal{C}_2}(V)$, the constrained problem (15) reformulates as $\min(f + g)$. We can now apply FISTA (Algorithm 3) to solve this problem with the gradient step given by (32) and the Lipschitz constant $L = 5$ and the proximal step $\text{prox}_{g/L}(U, V) = P_{\mathcal{C}_1}(U) + P_{\mathcal{C}_2}(V)$ given by (33)-(34).

3.5 Main algorithm

Having presented all the components of the hybrid algorithm, we now collect them in Algorithm 5, the main algorithm of the paper. The global convergence of Algorithm 5 is stated hereafter while its proof is deferred to Appendix B.

Theorem 2. *For any starting point $\beta^0 \in \mathbb{R}^{pT}$, the sequence $(\beta^n)_{n \geq 0}$ generated by Algorithm 5 converges to a global minimizer of F and the objective sequence $(F(\beta^n))_{n \geq 0}$ decreases to the minimum of F as the tolerance ϵ decreases to 0.*

4 Numerical experiments

4.1 Simulations: optimization performance

A simulation study was carried out to compare the proposed hybrid approach to SGFL with state-of-the-art optimization methods. The main focus here is on computational speed. Indeed, high-accuracy solutions are not needed in typical applications of SGFL; it is sufficient to correctly identify the optimal model segmentation and the sparsity structure of the minimizer of (9). Two sweeping patterns were examined for the hybrid approach: cyclical (HYB-C) and simple random sampling without replacement (HYB-R).

Benchmark methods. We provide a brief overview of the optimization methods used as benchmarks for the hybrid method. We refer the reader to the articles mentioned below for full details.

Algorithm 5 Sparse Group Fused Lasso

Input: Starting point $\beta^0 \in \mathbb{R}^{pT}$, regularization parameters $\lambda_1 \geq 0, \lambda_2 \geq 0$, tolerance $\epsilon > 0$

Output: β^n

```
progressDescent  $\leftarrow$  true, progressFusion  $\leftarrow$  true
n  $\leftarrow$  0
repeat
  while progressDescent = true do
    n  $\leftarrow$  n + 1
    Apply Algorithm 1 to  $\beta^{n-1}$  and output  $\beta^n$  {Block descent}
    if  $F(\beta^n) \geq (1 - \epsilon)F(\beta^{n-1})$  then
      progressDescent  $\leftarrow$  false
    end if
  end while
  while progressFusion = true do
    n  $\leftarrow$  n + 1
    Apply Algorithm 2 to  $\beta^{n-1}$  and output  $\beta^n$  {Fusion: single chains}
    if  $F(\beta^n) < (1 - \epsilon)F(\beta^{n-1})$  then
      progressDescent  $\leftarrow$  true, progressFusion  $\leftarrow$  true
    else
      progressFusion  $\leftarrow$  false
    end if
  end while
  if progressDescent = false and progressFusion = false then
    n  $\leftarrow$  n + 1
    Apply Algorithm 4 to  $\beta^{n-1}$  as in Section 3.3 and output  $\beta^n$  {Fusion: all chains}
    Apply Algorithm 3 to  $\beta^n$  as in Section 3.4 and output subgradient  $g \in \mathbb{R}^{pT}$ 
    if  $g \neq 0_{pT}$  then
      n  $\leftarrow$  n + 1
       $\alpha^* \leftarrow \operatorname{argmin}_{\alpha > 0} F(\beta^{n-1} - \alpha g)$ 
       $\beta^n \leftarrow \beta^{n-1} - \alpha^* g$  {Subgradient step}
    end if
  end if
until  $F(\beta^n) \geq (1 - \epsilon)F(\beta^{n-1})$ 
```

- *Smoothing proximal gradient* (SPG) Chen et al. (2012); Hadj-Selem et al. (2018); Kim and Xing (2012). This method deals with structured penalized regression problems where the penalty term admits a simple dual formulation, for example, group lasso and fused lasso. The idea of SPG is to add quadratic regularization to the dual expression of the penalty and to solve the smooth approximate problem by FISTA Beck and Teboulle (2009). In the context of SGFL, the objective (9) is approximated by

$\min_{\beta} \max_{\alpha} \left\{ \frac{1}{2} \sum_t \|X_t \beta_t - y_t\|_2^2 + \lambda_1 \sum_t \|\beta_t\|_1 + \lambda_2 \sum_t (\alpha'_t (\beta_{t+1} - \beta_t) - \mu \|\alpha_t\|_2^2) \right\}$ where $\beta \in \mathbb{R}^{pT}$, $\alpha \in \mathbb{R}^{p(T-1)}$, $\|\alpha_t\|_2 \leq w_t$ for all t , and $\mu > 0$ is a regularization parameter.

- *Primal-dual method* (PD) Condat (2013); Vũ (2013). This method pertains to the general convex optimization problem $\min_x f(x) + g(x) + (h \circ L)(x)$ where f is a smooth function, g and h are proximable functions, and L is a linear operator. In SGFL, f is taken to be the squared loss, g the lasso penalty, h the mixed $\ell_{2,1}$ norm, and L the first-order differencing operator. At each iteration, the algorithm essentially requires a few matrix-vector multiplications and two easy evaluations of proximal operators: soft-thresholding and projection on ℓ_2 balls.
- *Alternative direction of multipliers method* (ADMM). This widespread optimization method (see e.g. Boyd et al. (2011); Combettes and Pesquet (2011)) is suitable for convex programs of the form $\min_{x,z} f(x) + g(z)$ subject to linear constraints $Ax + Bz + c = 0$. The SGFL problem (9) can be expressed in this form by setting $x = \beta$, f equal to the squared loss plus lasso penalty, and $g(z) = \lambda_2 \sum_t w_t \|z_t\|_2$ where $z_t = \beta_{t+1} - \beta_t$ for $1 \leq t < T$. ADMM works by forming an augmented Lagrangian function $L_{\rho}(x, z, u) = f(x) + g(z) + \frac{\rho}{2} \sum_t \|u_t + z_t - (\beta_{t+1} - \beta_t)\|_2^2$ and optimizing it alternatively with respect to x (lasso problem) and to z (projection on ℓ_2 balls), along with closed-form updates of the dual variable u . The regularization parameter $\rho > 0$ must be selected by the user. Cao et al. (2018)
- *Linearized ADMM* (LADMM) Li et al. (2014). This technique is used in instances where one or both of the x - and z - updates in ADMM are computationally expensive. When applying ADMM to (9), one may linearize the squared loss and regularization term $\frac{\rho}{2} \sum_t \|u_t + z_t - (\beta_{t+1} - \beta_t)\|_2^2$ in the augmented Lagrangian L_{ρ} . This replaces the burdensome lasso problem (x -update) by a simple soft-thresholding operation.

Selection of tuning parameters. All the above methods have tuning parameters whose selection is nontrivial. In addition, the numerical performances of these methods are highly sensitive to their tuning parameters. We adopt the following strategies in the simulations.

- SPG. The parameter μ sets an upper bound on the gap between the minima of the original objective and its smooth approximation. However, suitably small values of μ yield unacceptably slow convergence. For this reason, we employ SPG with restarts, starting from a relatively large μ and decreasing it along a logarithmic scale when the algorithm fails to reduce the objective for 100 successive iterations.
- PD. Two proximal parameters τ, σ and a relaxation parameter ρ must be specified. Following the recommendations of the author of Condat (2013) (personal communi-

cation), we set $\rho = 1.9$, $\sigma = 0.25(1/\tau - \max_t \|X_t'X_t\|_2)$, and select τ from the grid $\{10^{-6}, 10^{-5}, \dots, 10^6\}$ by trial and error. Specifically, we run 100 iterations of the PD algorithm with $\tau = 10^{-6}$, $\tau = 10^{-5}$, and so on so forth until the best performance over 100 iterations decreases. (The best performance first increases with τ and then decreases).

- ADMM and LADMM. The regularization parameter ρ is selected by trial and error as above (best performance over 100 iterations) but going from large to small values: $\rho = 10^4, 10^3, \dots$

Simulation setup. We consider the piecewise multivariate linear regression model $y_t = X_t\beta_t + \varepsilon_t$ where β_t ($1 \leq t \leq T$) is constant on each segment $C_k = \{t : T_k \leq t < T_{k+1}\}$ ($1 \leq k \leq K$) with $T_k = \frac{(k-1)T}{K} + 1$ and $K = 10$. Two combinations of data dimensions were used: $(d, p, T) = (100, 500, 200)$ for a problem of moderate size (10^4 optimization variables) and $(d, p, T) = (100, 1000, 1000)$ for a larger problem (10^6 variables). Different correlation levels ρ_X in the predictor variables and noise levels σ_ε were examined. The predictors X_t were sampled from a multivariate normal distribution with mean zero, unit variance, and exchangeable correlation structure: $\text{Cor}((X_s)_i, (X_t)_j) = \rho_X$ if $(s, i) \neq (t, j)$ for $1 \leq s, t \leq T$ and $1 \leq i, j \leq p$. Note that correlation occurs both across components and across time. The regression vectors β_{T_k} were first obtained as independent realizations of $N(0_p, I_p)$, after which a fraction $s = 0.9$ of each vector was selected randomly and set to zero. As a result each β_t has sparsity level 0.9. The response vectors y_t were obtained by adding white noise $\varepsilon_t \sim N(0, \sigma_\varepsilon^2 I)$ to $X_t\beta_t$. The regularization parameters λ_1 and λ_2 were taken so that the SGFL solution $\hat{\beta}$ has the same change points and sparsity level as the true β . For each setup $(d, p, T, \rho_X, \sigma_\varepsilon)$, the simulation (data generation + optimization) was replicated 100 times if $(d, p, T) = (100, 500, 200)$ and 10 times if $(d, p, T) = (100, 1000, 1000)$.

The simulations were realized in the R programming environment R Core Team (2019) on a 24 Intel Xeon Gold processor with 46GB RAM (Ubuntu 18.04.4 LTS). The SPG, PD, ADMM, and LADMM methods were written in C++ using the Armadillo library Sanderson and Curtin (2016) and wrapped in R with `RcppArmadillo`. The proposed hybrid approach uses a mix of C++ and R; it is implemented in the R package `sparseGFL`. The package and simulation scripts are available at <https://github.com/ddegras/sparseGFL>. Each simulation was run on a single CPU core without parallelizing the execution of optimization methods.

The SPG, PD, ADMM, and LADMM methods were executed without stopping criterion for a number of iterations sufficient to reach convergence (3000-5000). The SPG used restarts as described above for 10^4 iterations at most. For the hybrid approach (HYB-C and HYB-R), the tolerance ϵ used in the stopping criterion of Algorithm 5 must be specified, as it determines not only the total number of iterations realized but also the type of optimization realized at each iteration (block coordinate descent, fusion cycle, etc.). It

was set to 10^{-6} to reflect the target relative accuracy of the solution to (9).

Results. The main performance measure used in the simulation study is the CPU runtime needed to reach a sufficiently accurate solution to (9). We select a target level of 10^{-6} for the relative accuracy of a solution $\hat{\beta} \in \mathbb{R}^{pT}$. That is, we deem a solution $\hat{\beta}$ to be sufficiently accurate if $F(\hat{\beta}) \leq (1 + 10^{-6}) \min_{\beta} F(\beta)$. This level of accuracy is sufficient to guarantee that a solution $\hat{\beta}$ has the same change points and (exactly or very nearly) the same sparsity structure as the minimizer β^* of F . For PD, ADMM, and LADMM, the initial time spent selecting suitable tuning parameters is included in the CPU runtime. (This initial time represents a relatively small fraction of the total runtime.) We point out that it is quite difficult to know good values of the tuning parameters *a priori* and that the performance of these three methods largely depends on their tuning parameters. Badly chosen tuning parameters may lead to excessively slow convergence or, in the other direction, to numerical overflow and divergence. If in a given simulation, an optimization method fails to reach a relative accuracy 10^{-6} , the total runtime of this method is reported.

The runtimes of the methods (to reach relative accuracy 10^{-6}) are summarized in Table 1. SPG is by far the slowest method, taking an order of magnitude more time than all other methods to converge. This method would likely perform better with more sophisticated or more finely tuned restarting rules than the one used here, for example Hadj-Selem et al. (2018). ADMM is the next slowest method and is not competitive for SGFL because of the necessity to solve a lasso problem at each iteration. PD and LADMM show comparable runtimes, with a very slight advantage for LADMM on problems of moderate size and a more marked advantage for PD on larger problems. Given that these are generic methods, their speed is quite satisfactory in comparison to the proposed hybrid method which is tailored for SGFL. In all setups, either HYB-C or HYB-R shows the best average runtime. HYB-R is the fastest method in about 56% of all simulations, HYB-C in 30%, LADMM in 9%, and PD in 5%. Unsurprisingly, HYB-R has a more variable runtime than HYB-C because of the additional randomization of the sweeping pattern. Interestingly, HYB-C performs best in the presence of correlation among predictor variables ($\rho_X \in \{0.10, 0.25\}$) whereas HYB-R shows superior performance when $\rho_X = 0$. The fact that HYB-C and HYB-R improve upon PD (the next best method) by respective speedup factors of 40% and 33% in the high-dimensional and correlated setup $p = 1000, T = 1000, \rho_X = 0.25$ is particularly promising for real world applications. See Figure 1 for an illustration.

We now turn to the accuracy of the methods, keeping in mind that the target accuracy is $F(\hat{\beta}) \leq (1 + 10^{-6}) \min_{\beta} F(\beta)$. Table 2 displays the worst-case accuracy of each method in each simulation setup. For a given method and setup, the worst-case accuracy is calculated as the quantile of level 99% of $F(\hat{\beta}) / \min_{\beta} F(\beta) - 1$ across all simulations. Therefore, values inferior to 10^{-6} in the table indicate that the target accuracy is virtually always met. It is important to remember that for HYB-C and HYB-R, the stopping tolerance $\epsilon = 10^{-6}$

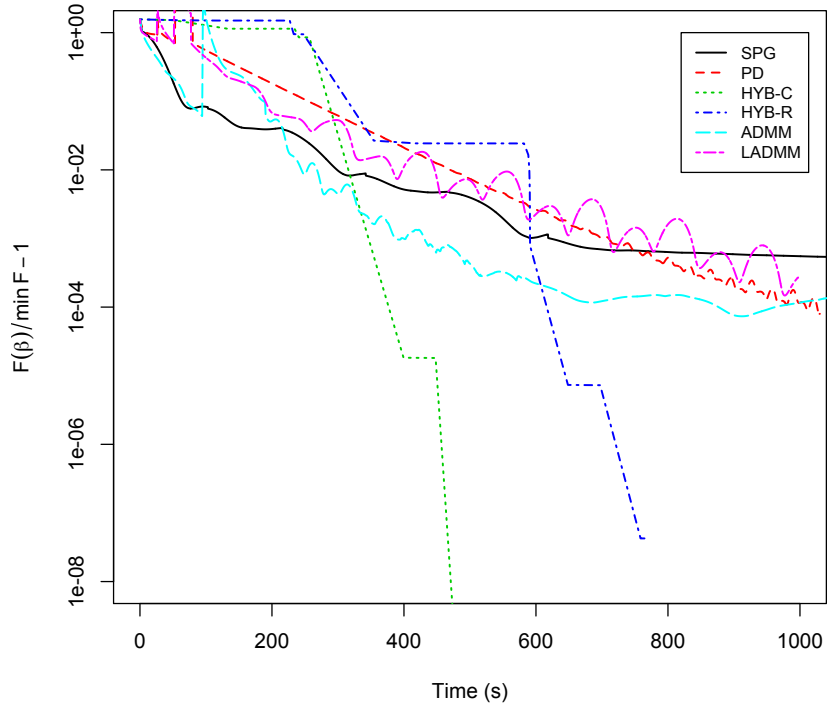


Figure 1: Simulation study: relative accuracy of solution versus CPU runtime in the high-dimensional setup $(d, p, T, \sigma_\varepsilon, \rho_X) = (100, 1000, 1000, 0, 0.25)$ (typical example).

Table 1: CPU runtime (in seconds) required to solve the SGFL problem (9) with relative accuracy 10^{-6} . Runtimes are averaged across 100 replications if $(d, p, T) = (100, 500, 200)$ and 10 replications if $(d, p, T) = (100, 1000, 1000)$. Best results are indicated in bold.

d	p	T	σ_ε	ρ_X	SPG	PD	HYB-C	HYB-R	ADMM	LADMM
100	500	200	0.00	0.00	225.7	31.7	26.7	22.3	46.7	28.1
100	500	200	0.25	0.00	212.0	31.8	26.3	22.3	46.7	28.4
100	500	200	2.50	0.00	174.8	30.8	27.9	23.1	45.2	27.4
100	500	200	5.00	0.00	210.8	31.5	16.9	17.1	50.8	28.3
100	500	200	0.00	0.10	173.4	35.7	30.8	45.5	51.4	40.7
100	500	200	0.00	0.25	176.1	50.4	38.0	48.2	76.8	52.1
100	500	200	0.25	0.25	177.6	48.6	37.1	48.4	69.4	47.1
100	1000	1000	0.00	0.00	6120.3	454.0	698.0	373.6	2261.5	971.8
100	1000	1000	0.00	0.25	7435.5	758.2	458.1	507.7	2384.6	879.0
100	1000	1000	0.25	0.25	6753.9	657.8	394.8	454.4	2376.3	893.8

is set to achieve the target accuracy level 10^{-6} , not to produce highly accurate solutions. Despite this fact, the worst-case accuracy of HYB-C is well below 10^{-6} in all setups and so is that of HYB-R (except for the high-noise setup $\sigma_\varepsilon = 5$). No other method achieves the target accuracy so consistently, although they run for a much longer time. Globally, HYB-C meets the target accuracy 10^{-6} in 100% of the simulations, HYB-R in 99.4%, ADMM in 96.2%, PD in 95.8%, LADMM in 95.1%, and SPG in 91.4%.

4.2 Simulations: statistical accuracy

In this part we assess the statistical accuracy of the SGFL in change point detection and parameter estimation. We also compare the SGFL to relevant methods for change point detection in high-dimensional linear regression listed below.

Benchmark methods.

- *Binary segmentation.* The binary segmentation algorithm (BSA) of Leonardi and Bühlmann (2016) is designed to detect change points and estimate sparse regression coefficients in high dimensional linear regression. It enjoys theoretical guarantees of consistency and convergence rates for the estimation of change points and regression coefficients. We note that the BSA is one of two estimation methods proposed in Leonardi and Bühlmann (2016). The other one utilizes dynamic programming and produces exact solutions to the statistical problem under study (unlike BSA) at the cost of much more intensive calculations.
- *Two-step approximation of SGFL.* The difficulty of the SGFL comes from the fact that it tackles time series segmentation (or change point detection) and sparse estimation of regression coefficients *simultaneously*. A simpler device would be to accomplish these tasks *sequentially*. We thus consider an approximate scheme that breaks the

Table 2: Relative accuracy: worst-case performance. For each method and each setup, the quantile of level 0.99 of $(F(\hat{\beta})/\min_{\beta} F(\beta)) - 1$ across all replications is displayed, where $\hat{\beta}$ is the final estimate produced by the method. For HYB-C and HYB-R, the optimization is stopped whenever the relative decrease in F between two successive iterations is less than 10^{-6} , whereas the other methods run for many iterations without stopping criterion. The numbers in the table must be compared to the target accuracy level 10^{-6} .

d	p	T	σ_{ε}	ρ_X	SPG	PD	HYB-C	HYB-R	ADMM	LADMM
100	500	200	0.00	0.00	5.7e-06	6.0e-15	1.9e-09	2.0e-09	1.3e-14	3.2e-12
100	500	200	0.20	0.00	8.8e-06	6.0e-15	1.7e-09	1.9e-09	9.1e-15	2.5e-10
100	500	200	2.50	0.00	4.1e-07	5.1e-15	2.6e-07	2.3e-07	6.2e-08	5.8e-09
100	500	200	5.00	0.00	6.6e-07	2.6e-10	7.5e-07	6.3e-04	1.8e-06	5.7e-07
100	500	200	0.00	0.10	6.8e-06	4.4e-07	2.7e-08	4.4e-08	2.7e-10	6.2e-10
100	500	200	0.00	0.25	2.0e-06	3.6e-04	3.1e-07	6.5e-07	2.3e-06	2.0e-05
100	500	200	0.25	0.25	5.6e-06	3.9e-04	2.2e-07	2.3e-07	1.2e-06	3.5e-05
100	1000	1000	0.00	0.00	8.1e-06	0.0e+00	1.8e-10	2.9e-10	1.3e-05	1.9e-06
100	1000	1000	0.00	0.25	5.9e-06	2.8e-04	9.6e-08	8.7e-07	3.3e-05	4.2e-04
100	1000	1000	0.25	0.25	5.3e-06	8.7e-04	1.7e-07	6.3e-08	2.3e-05	8.3e-05

SGFL in two steps (2S). The first step segments the time series by minimizing the SGFL objective (9) without lasso penalty ($\lambda_1 = 0$). As noted in Bleakley and Vert (2011), this can be efficiently implemented as a group lasso over the new variables $\theta_t = \beta_t - \beta_{t-1}$. In the second step, lasso regression is carried out over each segment obtained in the first step, yielding sparse estimates of the regression coefficients β_t . The two-step method is extremely efficient from a computational perspective, especially in view of fitting entire regularization paths. It also simplifies the selection of the regularization parameters λ_1 and λ_2 , which can be chosen separately in each step.

Simulation setup. The simulation framework of Section 4.1 was reused with different parameters. The data dimensions were set to $(d, p, T) = (20, 200, 100)$ (moderate dimension) or $(d, p, T) = (100, 500, 200)$ (high dimension). The change points were set to $\{0.2T + 1, 0.5T + 1, 0.9T + 1\}$ (few change points with one near the boundary) or $\{0.2T + 1, 0.4T + 1, 0.6T + 1, 0.8T + 1\}$ (equispaced change points with higher density). Due to high computational load, only the 3-change points scenario was considered in high dimension. The noise level σ_{ε} was either 0.25 (low noise) or 1 (moderate noise). The sparsity level of the regression vectors β_t was set to $s = 0.99$. The predictors X_t were generated independently ($\rho_X = 0$). Qualitatively similar results were obtained with different levels of signal sparsity, noise variance, and predictor correlation. They are provided as

Supplementary Materials.

The BSA has several tuning parameters: the maximum number k_{max} of segments allowed (set to 10), the minimum distance δ between change points (set to 0.1 on a unit interval), and a regularization parameter λ for lasso regression. The two-step method and the SGFL require two regularization parameters: λ_1 (lasso penalty) and λ_2 (total variation penalty). To our knowledge no selection method with theoretical guarantees has yet been developed for our particular context (high-dimensional regression with multiple change points). We also note that (i) applying cross-validation techniques in this context is methodologically and computationally difficult, and (ii) in high dimension the usual Akaike Information Criterion (AIC) and Bayesian Information Criterion (BIC) tend to not penalize enough model complexity and lead to overfitting the data (e.g. Chen and Chen (2008); also confirmed in simulations). For these reasons we utilize a high-dimensional version of BIC to select $\lambda, \lambda_1, \lambda_2$ (HBIC, Wang and Zhu (2011)). Ignoring irrelevant additive constants, this criterion can be formulated as

$$\begin{aligned} \text{HBIC}(\lambda) = dT \log \left(\sum_{t=1}^T \|y_t - X_t \hat{\beta}_t(\lambda)\|^2 \right) \\ + 2\gamma \log(p) \quad (\# \text{ free parameters in } \hat{\beta}(\lambda)) \end{aligned} \quad (35)$$

where λ denote all regularization parameters and $\gamma \geq 1$ must be specified. The number of free parameters is the total number of nonzero coefficients in the vectors $\hat{\beta}_t$ associated with change points, or equivalently the number of nonzero coefficients in the increments $\theta_t = \beta_t - \beta_{t-1}$ with $\beta_0 = 0_p$. The choice of a value γ that produces good estimates $\hat{\beta}$ is in itself a difficult problem; in practice, both λ and γ should be considered as regularization parameters to select. Values $\gamma \in \{1, 2, \dots, 10\}$ were used in the simulations to assess the effect of this parameter.

For each combination of change points and noise level, the simulation was replicated 100 times. In each replication, the BSA, two-step method, and SGFL method were fitted to the data over a fine grid of regularization parameters. (Between 10 and 100 values were considered for each grid, depending on the sensitivity of the parameter λ, λ_1 , or λ_2 and on the computational requirements of the estimation method. The largest grid value was obtained by theoretical considerations to make the estimate uniformly zero or time-invariant; the smallest grid value was taken as a sufficiently small ratio of the largest, between 0.1 and 0.001. Grid values were equispaced on a linear or logarithmic scale as required.) For each estimation method and value γ , the estimate $\hat{\beta}(\lambda)$ minimizing (35) as a function of λ was determined. The best estimate $\hat{\beta}(\lambda)$ with regards to change point detection was also determined, more precisely the one minimizing the Hausdorff distance between the estimated and the true change points. For reference, the Hausdorff distance

between two non empty subsets X and Y of a metric space (M, d) is

$$d_H(X, Y) = \max \left(\sup_{x \in X} \inf_{y \in Y} d(x, y), \sup_{y \in Y} \inf_{x \in X} d(x, y) \right).$$

We note that the two methods used to select the regularization parameters λ or (λ_1, λ_2) are infeasible in practice as they exploit information on the true regression coefficients β . These methods are meant to describe the estimation performance when a good value γ is used in (35) (for the first method) and when the change points are estimated with high accuracy (for the second). In a controlled simulation environment, this makes it possible to ignore the uncertainty associated with selecting regularization parameters and to compare estimation methods at their best performance level.

Results. Table 3 reports simulation results for all configurations of model dimension, change points, noise level and for all estimation methods (BSA, 2S, SGFL). In each simulation setup, the results are averaged across 100 replications. The performance measures in each column are the number of estimated change points (NCP), the Hausdorff distance between estimated and true change points (d_H), the true positive rate and positive predictive value in detecting nonzero regression coefficients (TPR, PPV), the sparsity level of the estimate (\hat{s}), and a pseudo R^2 coefficient.

In the column NCP, perfect detection would yield $\text{NCP} = 3$ in the case where the change points are $\{0.2T + 1, 0.5T + 1, 0.9T + 1\}$ and $\text{NCP} = 4$ in the case $\{0.2T + 1, 0.4T + 1, 0.6T + 1, 0.8T + 1\}$. In the column d_H , the best possible value is zero and the worst is T (when no change point is detected). The true positive rate TPR (also called sensitivity) is the proportion of nonzero coefficients in β detected by a method. (There were $(1 - s)pT$ nonzero coefficients in β .) The predictive positive value PPV (also called specificity) is the proportion of nonzero coefficients in $\hat{\beta}$ that are truly nonzero in β . The sparsity level \hat{s} of an estimate $\hat{\beta}$ should be close to the sparsity $s = 0.99$ of the true β . The pseudo R^2 measures goodness of fit and is calculated as $R^2 = 1 - (\sum \|y_t - X_t \hat{\beta}_t\|^2 / \sum \|y_t - \bar{y}\|^2)$.

The column λ of Table 3 refers to the selection method for λ . The method based on the Hausdorff distance (d_H) has been discussed before. Estimation performance with the HBIC selection method corresponds to the “best” possible choice of $\gamma \in \{1, 2, \dots, 10\}$ defined as follows. For each estimation method, replication, and value γ , the estimate $\hat{\beta}(\lambda)$ minimizing the HBIC (35) was determined and the corresponding measures NCP, ..., R^2 in Table 3 were calculated. A composite score giving equal weight to each measure was constructed to reflect best overall performance. Specifically, each measure was linearly transformed to produce the value zero as best performance (e.g. NCP equal to the true number of change points, $d_H = 0$, TPR = 1, $\hat{s} = s$) and the value one as worst performance. The results displayed in the table are for the value γ with minimum average composite score across replications.

Looking at Table 3, it appears that the BSA performs extremely well in low noise situations ($\sigma_\varepsilon = 0.25$) both in the 3- and 4- change point scenarios (see HBIC rows). The method accurately detects all change points while simultaneously recovering nearly all nonzero coefficients of β , attaining a sparsity level very close to the target 0.99, and achieving a very high R^2 coefficient. However this high performance seems to break down in moderate noise situations ($\sigma_\varepsilon = 1.0$). There, the method largely fails to estimate the number of change points and their locations; the sparsity of its estimates falls to about 0.5-0.6 and the PPV falls correspondingly to 0.03. The rows BSA/ d_H in the table reveal that the BSA can in fact accurately locate the change points for a suitable choice of λ . But even for this choice of λ , the estimate $\hat{\beta}$ keeps a low sparsity (0.63 or 0.65) and extremely low PPV (0.04). It is worth noting that in less sparse regression models ($s = 0.9$ instead of $s = 0.99$), the BSA shows good statistical performance at all noise levels (see Supplementary Materials for details).

The two-step method (2S) performs remarkably well with respect to all performance measures in all simulation setups. Its performance degrades in the moderate noise setup with 4 change points but remains at an acceptable level. Concerning the estimation of sparsity patterns in β , this method consistently achieves a high TPR and high PPV (at least in low noise: between 0.90 and 0.93). The SGFL performs very well in change point detection but less so in parameter estimation (its TPR and PPV stay between 0.73 and 0.89 in all setups) and goodness of fit. Its performance is very stable in all change point configurations and noise levels; in particular, its sparsity level stays at the target level 0.99 throughout. Additional simulations showed that this method can still accurately detect change points under high noise levels ($\sigma_\varepsilon = 2.5$).

In comparison to the moderate dimension setup $(d, p, T) = (20, 200, 100)$, the statistical performance of methods does not seem to degrade in the high dimension setup $(d, p, T) = (100, 500, 200)$. One possible explanation is that while the number of change points remain essentially in the two setups, i.e. 3, the associated time segments where the regression vectors are constant are twice as long when $T = 200$, which makes the detection of change points easier.

We conclude this section with remarks on the HBIC and on computations. Regarding HBIC, the statistical performance all estimation methods is not very sensitive to γ in low noise but it is very much so in moderate-to-high noise. In the latter case, the HBIC may be too stringent as the best performance of estimation methods is attained at the boundary value $\gamma = 1$. Concerning speed and scalability, the 2S method was an order of magnitude faster than the BSA and SGFL in the simulations. In the moderate dimension setting, it took on average between 15 s and 20 s to calculate $\hat{\beta}(\lambda_1, \lambda_2)$ over a dense grid (100 values for λ_1 , 20 for λ_2) versus 290-370 s for SGFL (30 values for λ_1 , 20 for λ_2) and 510-570 s for BSA (20 values for λ). In the high dimension setting, 2S ran in a few minutes, SGFL in 2-3 hours, and BSA in about 5-6 hours. Detailed runtime information can be found in the

Table 3: Simulations: statistical accuracy. Columns indicate the simulation setup, estimation method, selection method for regularization parameters, number of estimated change points, Hausdorff distance between estimated and true change points, true positive rate and positive predictive value in detecting nonzero regression coefficients, sparsity level (target level $s = 0.99$), and pseudo- R^2 . Results are averaged over 100 replications (standard deviation in brackets). For the HBIC selection method, the best results are in bold.

Setup	Method	λ	NCP	d_H	TPR	PPV	\hat{s}	R^2
$d = 20$ $p = 200$ $T = 100$ $\sigma_\varepsilon = 0.25$ {21, 51, 91}	BSA	HBIC	3.1 (0.3)	0.5 (2.2)	0.97 (0.06)	0.77 (0.32)	0.98 (0.03)	0.95 (0.03)
	2S	HBIC	3.8 (0.8)	1.9 (6.2)	0.93 (0.10)	0.93 (0.06)	0.99 (0.00)	0.95 (0.03)
	SGFL	HBIC	3.0 (0.2)	1.1 (6.3)	0.89 (0.12)	0.83 (0.11)	0.99 (0.00)	0.90 (0.03)
	BSA	d_H	3.0 (0.2)	0.3 (1.7)	0.98 (0.05)	0.77 (0.32)	0.98 (0.04)	0.95 (0.03)
	2S	d_H	4.0 (1.0)	0.9 (1.0)	0.95 (0.08)	0.97 (0.04)	0.99 (0.00)	0.91 (0.06)
	SGFL	d_H	3.0 (0.0)	0.0 (0.0)	0.91 (0.11)	0.92 (0.15)	0.99 (0.01)	0.82 (0.10)
$d = 20$ $p = 200$ $T = 100$ $\sigma_\varepsilon = 1.00$ {21, 51, 91}	BSA	HBIC	1.5 (1.4)	51.5 (43.4)	0.94 (0.09)	0.03 (0.03)	0.58 (0.2)	0.50 (0.25)
	2S	HBIC	5.5 (3.8)	26.2 (20.2)	0.72 (0.19)	0.71 (0.14)	0.99 (0.00)	0.51 (0.19)
	SGFL	HBIC	2.7 (0.6)	11.4 (20.2)	0.77 (0.16)	0.73 (0.19)	0.99 (0.01)	0.48 (0.17)
	BSA	d_H	3.3 (0.6)	2.9 (4.2)	0.96 (0.07)	0.04 (0.03)	0.63 (0.17)	0.68 (0.09)
	2S	d_H	10.6 (5.0)	12.0 (5.8)	0.73 (0.16)	0.81 (0.13)	0.99 (0.00)	0.48 (0.16)
	SGFL	d_H	3.2 (0.6)	0.8 (2.2)	0.8 (0.16)	0.70 (0.38)	0.92 (0.20)	0.43 (0.16)
$d = 20$ $p = 200$ $T = 100$ $\sigma_\varepsilon = 0.25$ {21, 41, 61, 81}	BSA	HBIC	4.0 (0.2)	0.1 (1.0)	0.96 (0.06)	0.80 (0.26)	0.98 (0.02)	0.96 (0.02)
	2S	HBIC	5.6 (1.3)	2.2 (3.3)	0.92 (0.09)	0.93 (0.04)	0.99 (0.00)	0.95 (0.03)
	SGFL	HBIC	4.0 (0.2)	0.8 (3.9)	0.88 (0.11)	0.74 (0.14)	0.99 (0.00)	0.90 (0.04)
	BSA	d_H	4.0 (0.2)	0.1 (1.0)	0.96 (0.06)	0.80 (0.26)	0.98 (0.02)	0.96 (0.02)
	2S	d_H	5.7 (1.4)	1.9 (2.3)	0.94 (0.08)	0.96 (0.05)	0.99 (0.00)	0.92 (0.06)
	SGFL	d_H	4.0 (0.3)	0.2 (1.2)	0.87 (0.10)	0.95 (0.15)	0.99 (0.01)	0.81 (0.08)
$d = 20$ $p = 200$ $T = 100$ $\sigma_\varepsilon = 1.0$ {21, 41, 61, 81}	BSA	HBIC	1.7 (2.1)	62.3 (41.8)	0.94 (0.07)	0.03 (0.04)	0.54 (0.21)	0.42 (0.28)
	2S	HBIC	7.5 (2.9)	11.1 (10.4)	0.69 (0.18)	0.76 (0.10)	0.99 (0.00)	0.55 (0.16)
	SGFL	HBIC	3.6 (0.6)	8.1 (10.2)	0.74 (0.15)	0.76 (0.21)	0.99 (0.01)	0.47 (0.16)
	BSA	d_H	5.7 (2.1)	4.8 (4.7)	0.95 (0.06)	0.04 (0.04)	0.65 (0.17)	0.74 (0.06)
	2S	d_H	10 (3.3)	6.1 (3.0)	0.75 (0.14)	0.82 (0.12)	0.99 (0.00)	0.52 (0.14)
	SGFL	d_H	4.1 (0.5)	0.8 (1.8)	0.84 (0.13)	0.55 (0.42)	0.83 (0.29)	0.46 (0.14)
$d = 100$ $p = 500$ $T = 200$ $\sigma_\varepsilon = 0.25$ {41, 101, 181}	BSA	HBIC	3.0 (0.0)	0.0 (0.0)	0.98 (0.03)	1.00 (0.02)	0.99 (0.00)	0.99 (0.00)
	2S	HBIC	3.0 (0.2)	0.0 (0.2)	0.98 (0.03)	0.99 (0.01)	0.99 (0.00)	0.99 (0.00)
	SGFL	HBIC	3.0 (0.1)	0.6 (6.0)	0.96 (0.05)	0.52 (0.04)	0.98 (0.00)	0.96 (0.00)
	BSA	d_H	3.0 (0.0)	0.0 (0.0)	0.99 (0.02)	1.00 (0.02)	0.99 (0.00)	0.99 (0.00)
	2S	d_H	3.0 (0.2)	0.0 (0.2)	0.98 (0.03)	1.00 (0.01)	0.99 (0.00)	0.98 (0.01)
	SGFL	d_H	3.0 (0.0)	0.0 (0.0)	0.90 (0.08)	0.94 (0.04)	0.99 (0.00)	0.89 (0.05)
$d = 100$ $p = 500$ $T = 200$ $\sigma_\varepsilon = 1.0$ {41, 101, 181}	BSA	HBIC	3.2 (0.4)	4.0 (8.0)	0.99 (0.02)	0.08 (0.06)	0.84 (0.08)	0.83 (0.04)
	2S	HBIC	3.1 (0.3)	0.1 (0.3)	0.94 (0.06)	0.97 (0.02)	0.99 (0.00)	0.82 (0.04)
	SGFL	HBIC	3.0 (0.0)	0.0 (0.1)	0.92 (0.07)	0.75 (0.08)	0.99 (0.00)	0.79 (0.04)
	BSA	d_H	3.2 (0.4)	4.0 (8.0)	0.99 (0.02)	0.08 (0.06)	0.84 (0.08)	0.83 (0.04)
	2S	d_H	3.1 (0.3)	0.1 (0.3)	0.95 (0.05)	0.99 (0.02)	0.99 (0.00)	0.81 (0.04)
	SGFL	d_H	3.0 (0.0)	0.0 (0.0)	0.89 (0.07)	0.94 (0.05)	0.99 (0.00)	0.74 (0.05)

Supplementary Materials.

4.3 Air quality data

We illustrate the SGFL with an application to air quality monitoring. The dataset used in this example was analyzed in De Vito et al. (2008, 2009) and is available on the UCI Machine Learning Repository (<https://archive.ics.uci.edu/ml//datasets/Air+quality>). It contains 9357 instances of hourly averaged responses from an array of 5 metal oxide chemical sensors embedded in an Air Quality Chemical Multisensor Device. Data were recorded from March 2004 to February 2005 on a device located in a significantly polluted area, at road level, within an Italian city. Ground truth hourly averaged concentrations for carbon monoxide (CO), Non Metanic Hydrocarbons (NMHC), Benzene (C6H6), Total Nitrogen Oxides (NOx) and Nitrogen Dioxide (NO2) were provided by a co-located reference certified analyzer. As described in De Vito et al. (2008), the data show evidence of cross-sensitivity as well as of concept and sensor drift, which ultimately affects the sensors' capability to estimate pollutant concentration.

The hourly averaged measurements of the 4 target pollutants, 5 chemical sensors, and 3 meteorological variables (temperature, relative humidity, and absolute humidity) are displayed in Figure 2 after shifting and scaling to facilitate visualization. In the statistical analysis, all variables have been centered and scaled. Time points with missing values have been ignored, which reduced the time series length to $T = 6930$. Because of this, the quantitative results of this analysis should be interpreted with some caution. (A follow-up analysis, wherein missing values were replaced by the last observed value carried forward, produced roughly the same number of segments as in the present analysis with slight differences in change point location. The regression coefficients were very similar but the goodness of fit was much lower on the imputed dataset.) Correlation patterns between variables are depicted in Figure 3.

The main goals in this application are to: (i) calibrate the sensors so that they accurately estimate the true pollutant concentrations, and (ii) determine how often the sensors must be recalibrated in order to maintain a high accuracy. Here we use SGFL in an exploratory way to determine which sensors and weather variables are predictive of the true pollutant levels, and how the regression relationship evolves over time. The relationship between the study variables is conveniently expressed as

$$y_t = A_t x_t + \varepsilon_t \tag{36}$$

where $y_t \in \mathbb{R}^d$ represents the true pollutant concentrations at time t , $x_t \in \mathbb{R}^m$ the sensor measurements and weather variables, and $A_t \in \mathbb{R}^{d \times m}$ the unknown regression coefficients with $d = 4$ and $m = 8$ or $m = 9$ if the model contains an intercept. This model can be recast in the form $y_t = X_t \beta_t + \varepsilon_t$ considered throughout the paper by setting $\beta_t = \text{vec}(A_t)$ (concatenate the columns of A_t) and $X_t = (x_t') \otimes I_d$ (Kronecker product). However with this formulation the matrix $X_t \in \mathbb{R}^{d \times dm}$ becomes large and sparse, which tends to slow down calculations. For computational speed and user convenience, the R package `sparseGFL` has

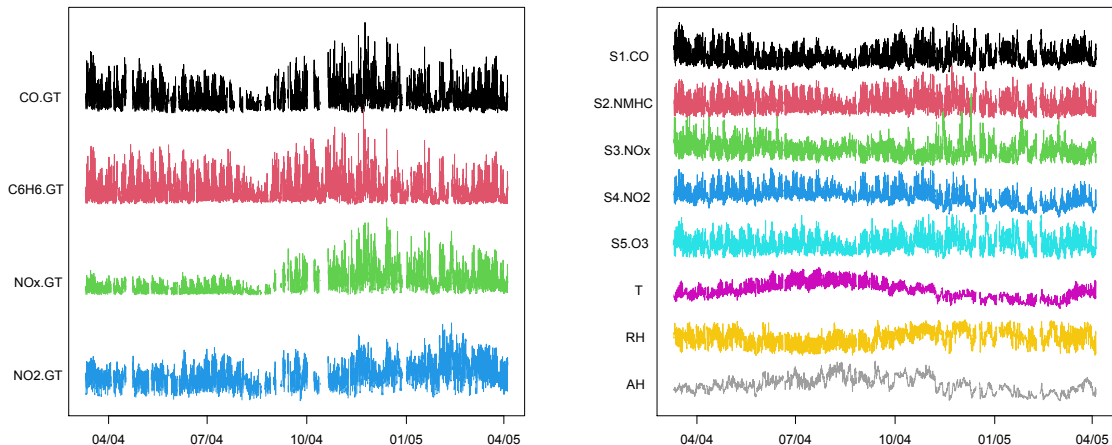


Figure 2: Air quality data. Left: pollutant levels (ground truth). Right: sensor measurements and meteorological variables. After each sensor number S1, S2, ... is the pollutant nominally targeted by this sensor.

dedicated functions for both models (1) and (36).

Model fitting. The main model considered in the data analysis is (36) with x_t containing all sensor measurements, weather variables, plus an intercept ($m = 9$, $p = dm = 36$). For comparison, we have also examined the corresponding time-invariant model $y_t = Ax_t + \varepsilon_t$ as well as a much more complex piecewise regression model containing all sensor measurements, lagged versions thereof, weather variables, and interaction terms. (This model had $p = 156$ regression coefficients per time point, that is, about 1 million optimization variables.) The motivation for this model was to investigate whether exploiting sensor measurements from the recent past could enhance estimation accuracy and whether weather conditions did modulate the regression relationship between sensors and targets. Our results were inconclusive with regards to these questions and because the complex model did not decisively improve upon the main-effects-only model, we did not pursue it further. We thus focus on model (36) with $m = 9$ predictors and on the time-invariant model.

The time-invariant regression model was fitted to the data by ordinary least squares (OLS). The SGFL was fitted with Algorithm 5 over a lattice of regularization parameters (λ_1, λ_2) spanning several orders of magnitudes: $[10^{-4}, 1]$ for λ_1 and $[5, 200]$ for λ_2 . The total variation weights w_t in (9) were set to 1 and a small ridge regression penalty was added to the lasso penalty to stabilize the estimation (mixing coefficient $\alpha = 0.9$ in (38)). For

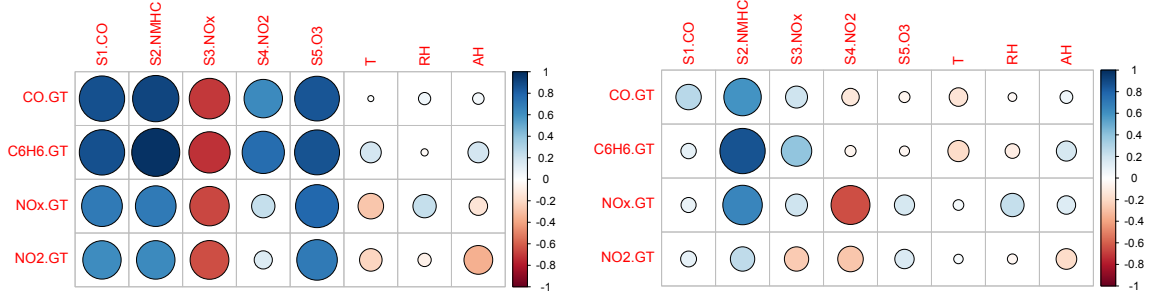


Figure 3: Air quality data: correlation between pollutant levels and predictors. Left: full correlation. Almost all sensors are strongly correlated to all true pollutant concentrations. This correlation is positive as expected for all sensors except for S3.NOx, which is surprising. Right: partial correlation. S2.NMHC is by far the strongest predictor of all pollutant levels (in equality with S4.NO2 for the target NOx. Interestingly none of the sensors is the best predictor for the pollutant it nominally targets.

each (λ_1, λ_2) , after calculating the SGFL solution $\tilde{A} = \tilde{A}(\lambda_1, \lambda_2) \in (\mathbb{R}^{d \times m})^T$, segments of length less than 72 time points (3 days) were fused with contiguous longer segments. For each segment $C_k = \{t : T_k \leq t < T_{k+1}\}$, the matrix A_{T_k} was re-estimated by OLS while preserving the zero coefficients of \tilde{A}_{T_k} : $\min_{A_{T_k}} \frac{1}{2} \sum_{t \in C_k} \|A_{T_k} x_t - y_t\|_2^2$ subject to $(A_{T_k})_{ij} = 0$ if $(\tilde{A}_{T_k})_{ij} = 0$. This re-estimation step is common in penalized regression and reduces the bias induced by the penalty. We denote by SGFL-OLS this two-stage estimation procedure and by $\hat{A} = \hat{A}(\lambda_1, \lambda_2)$ the associated estimator.

The best SGFL-OLS solution $\hat{A}(\lambda_1, \lambda_2)$ was taken as the one minimizing the BIC score (additive constants omitted)

$$\text{BIC}(\lambda_1, \lambda_2) = dT \log \left(\sum_{t=1}^T \|y_t - \hat{A}_t(\lambda_1, \lambda_2) x_t\|^2 \right) + \log(dT) \quad (\# \text{ free parameters in } \hat{A}(\lambda_1, \lambda_2)) \quad (37)$$

with the number of free parameters calculated as in Section 4.2. BIC (or AIC) are appropriate selection methods here because of the low-dimensional setting $p \ll T$.

Results. Due to the close connection between partial correlation and multiple regression, the time-invariant regression estimate $\hat{A} = (YX')(XX')^{-1} \in \mathbb{R}^{4 \times 9}$ is qualitatively comparable to the partial correlation matrix of Figure 3. In model (36) with $m = 9$ predictors (sensors, weather variables, intercept), the optimal SGFL-OLS solution $\hat{A}(\lambda_1, \lambda_2)$ for the BIC (37) is obtained for $(\lambda_1, \lambda_2) = (0.0060, 50)$. This solution has a sparsity level of 8.6% and overall R^2 of 94.3%. It segments the time range $\{1, \dots, T\}$ into $K = 23$ segments.

(The AIC solution corresponds to $(\lambda_1, \lambda_2) = (0.0060, 40)$. It is similar to the BIC solution but slightly less sparse and with more segments: 35.)

Table 4 reports the R^2 coefficient of each fitted model for each pollutant. For the time-invariant model, this measure varies from 0.756 for NO2 to 0.974 for C6H6. Although the piecewise model (36) improves upon the time-invariant model by 7.8% overall in terms of R^2 , more sophisticated methods may be required to capture the nonlinear component of the relationship between target pollutants and sensors, e.g. neural network architectures as in De Vito et al. (2009).

Table 4: Air quality data: goodness of fit (R^2) of multivariate linear regression models. The time-invariant model is fitted by ordinary least squares. The piecewise model (36) is estimated by solving the SGFL (9) for a range of values (λ_1, λ_2) and selecting the solution that minimizes the BIC score (37).

Regression model	CO	C6H6	NOx	NO2
Time-invariant	0.886	0.974	0.842	0.758
Time-varying	0.941	0.992	0.943	0.897

Figure 4 shows the five largest regression coefficients (by average magnitude) of the SGFL-OLS solution over time. Only sensor-related coefficients are displayed there, but temperature and absolute humidity are also strong predictors of the target pollutant levels. The associated pairs of sensors and targets are also strongly related in the time-invariant regression model (see Figure 3). The figure reveals that this regression relationship varies considerably over time, which justifies the need for regularly recalibrating the sensors. Although the changes in regression are mostly smooth over time, they can sometimes be very abrupt and large in magnitude. These observations must however be tempered by the fact that other SGFL-OLS estimates $\hat{A}(\lambda_1, \lambda_2)$ can fit the data nearly as well as the BIC solution with far fewer segments. For example, a highly parsimonious SGFL-OLS estimate can attain an overall $R^2 = 0.910$ while producing only $K = 4$ segments of average length 72 days.

In conclusion of this example, the SGFL-OLS methodology combined with BIC selection suggests that the linear relationship between pollutant levels and sensor measurements stays homogenous over segments of about one week. This scale is consistent with the observation in De Vito et al. (2009) that the optimal training period for neural network-based predictive models is 10 days, after which no improvement in performance is observed. Also, to give perspective on the accuracy of SGFL-OLS in this example, we note that its mean absolute error in estimating the NO2 level is $11.2 \mu\text{g}/\text{m}^3$ (NO2 is the most difficult of the 4 pollutants to predict as Table 4 shows). The best mean absolute error for NO2 with a neural network in De Vito et al. (2009) is $19.8 \mu\text{g}/\text{m}^3$. These results are encouraging although the two figures are not directly comparable. Indeed our approach continuously adjusts the

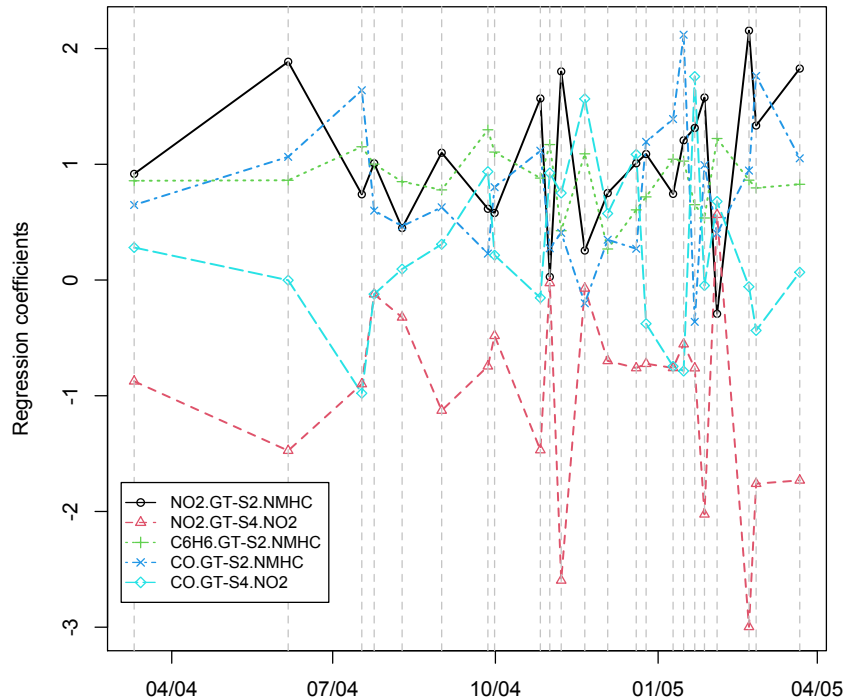


Figure 4: Air quality data: time-varying regression coefficients and model segmentation obtained by SGFL. For clarity, the piecewise-constant coefficients are represented with continuous lines rather than step functions.

regression model using both sensor and pollutant data whereas De Vito et al. (2009) makes predictions for most of the observation period using only sensor readings.

5 Discussion

This paper has introduced the sparse group fused lasso (SGFL) as a statistical paradigm for segmenting regression models in the context of high-dimensional time series. The objective function used in SGFL favors sparsity in regression coefficients via a lasso penalty and parsimony in the number of segments or change points via an ℓ_2 total variation penalty. This combination of penalties is essential for model segmentation in high dimension and has very rarely been studied in the literature. More common variants of fused lasso based

on ℓ_1 total variation penalties are not appropriate for this purpose.

A hybrid algorithm has been developed to optimize the SGFL objective function, which is a highly nontrivial problem of nonsmooth and nonseparable convex optimization. This algorithm exploits the problem’s structure by operating at different levels (block, single fusion chain, all fusion chains, all blocks) with optimization techniques such as block coordinate descent and subgradient methods. With its ability to perform local or global, aggregating or splitting iterations, the hybrid algorithm can flexibly explore the search space but also “lock in” a given model segmentation and make extremely fast progress. In addition to its computational speed, the hybrid algorithm bears the advantage of not requiring any complicated selection of tuning parameters, which renders it more accessible to non-expert users.

In our simulations, the proposed algorithm has realized significant speed gains in comparison to state-of-the-art techniques like ADMM and primal-dual methods. The speedup was particularly important in high-dimensional situations with millions of optimization variables (30%-40% speedup), which is particularly encouraging in view of large scale applications. With regards to statistical accuracy, the SGFL has shown reasonable performance in recovering nonzero regression coefficients although competing methods were more accurate. It performed extremely well in change point detection, even at high noise levels, which the other methods could not achieve. A simplified two-step version of the SGFL has shown excellent computational speed and accuracy in the recovery of sparsity patterns as well as very good performance in change point detection (at least in low to moderate noise). This simplified approach emerges as an interesting alternative to SGFL and is certainly worthy of further investigation. The practical effectiveness of the SGFL has been illustrated with the analysis of air quality data, which has given insights on the frequency of changes in the relationship between sensor readings and target pollutant levels and on the attainable prediction performance. A challenge in our simulations and data analyses using SGFL was the selection of regularization parameters (λ_1, λ_2) . While the standard AIC/BIC lead to overfitting the data in multiple instances (i.e. too many change points and/or too many nonzero regression coefficients), the alternative selection criterion we found, HBIC, seemed overly conservative in moderate to high noise. In addition, the HBIC itself requires selecting an extra regularization parameter (γ) . Theoretical investigations of the asymptotics of SGFL and more numerical experimentation will be needed to find suitable selection methods.

The hybrid method for the SGFL is implemented in the R package `sparseGFL` available at <https://github.com/ddegras/sparseGFL>.

Extensions

Elastic net penalty. The sparse group fused lasso can be extended to encompass an *elastic net* penalty (Zou and Hastie (2005)):

$$\min_{\beta \in \mathbb{R}^{pT}} \left\{ \frac{1}{2} \sum_{t=1}^T \|y_t - X_t \beta_t\|_2^2 + \lambda_1 \sum_{t=1}^T \left(\alpha \|\beta_t\|_1 + \frac{(1-\alpha)}{2} \|\beta_t\|_2^2 \right) + \lambda_2 \sum_{t=1}^{T-1} w_t \|\beta_{t+1} - \beta_t\|_2 \right\}. \quad (38)$$

The elastic net penalty combines the lasso penalty and the (squared ℓ_2) ridge regression penalty thanks to a mixing coefficient $\alpha \in [0, 1]$ ($\alpha = 1$ corresponds to pure lasso, $\alpha = 0$ to pure ridge). This penalty seeks the “best of both worlds”, namely the sparsity-inducing effect of the lasso and the stabilization effect of ridge regression. In particular the ridge penalty can mitigate the adverse effects of high correlation among predictors in lasso. Also, from a theoretical perspective, when $\alpha < 1$, the objective function F is strictly convex and thus admits a unique minimizer.

Loss function. For simplicity of exposition, we have developed the SGFL and hybrid optimization method in the context of linear regression. However, they are by no means restricted to linear regression: the squared loss in the objective function (9) can be replaced by any differentiable loss function. For example, our methodology can be used for classification problems using exponential, logistic, or generalized smooth hinge loss functions.

Future lines of research

Pathwise implementation of SGFL. In practice, one rarely solves the SGFL for a single pair of regularization parameters (λ_1, λ_2) but rather along a path of values. The selection of such path is in itself a nontrivial problem for two main reasons: first the interplay between λ_1 and λ_2 in the lasso and total variation penalty and second, the computation time required to fit the SGFL. To elaborate on the first point, for a given λ_1 , varying λ_2 may not only affect the number of segments produced by the SGFL solution $\hat{\beta} = \hat{\beta}(\lambda_1, \lambda_2)$ but also the sparsity of this solution. Conversely, for fixed λ_2 , varying λ_1 may not affect only the sparsity of the solution but also the model segmentation.

One strategy may be to calculate regularization paths over a product grid $G = G_1 \times G_2$. The problem then is to determine ranges and sizes for G_1 and G_2 that yield a sufficiently fine-grained path of solutions $\hat{\beta}(\lambda_1, \lambda_2)$ with a good variety of sparsity levels and segmentations while keeping the computational load reasonable. The largest value in G_1 , say $\lambda_{1\max}$, can be determined analytically, for example as $\lambda_{1\max} = \frac{1}{T} \|\sum_{t=1}^T X_t' y_t\|_\infty$, so that for

$\lambda_2 = \infty$ (time-invariant solution) $\hat{\beta}(\lambda_1, \infty) \equiv 0$ if and only if $\lambda_1 \geq \lambda_{1\max}$. One can then take G_1 as an equispaced grid on a linear or logarithmic scale going from $\lambda_{1\max}$ to a small fraction of $\lambda_{1\max}$, say 0.001 or 0.0001. The question remains to select a suitable grid G_2 . More precisely, for a given $\lambda_1 \in G_1$, it would be useful to know the smallest $\lambda_2 = \lambda(\lambda_1)$ such that $\hat{\beta}(\lambda_1, \lambda_2) = \hat{\beta}(\lambda_1, \infty)$, say $\lambda_{2\max}(\lambda_1)$. With this information, one can avoid wasting time solving (9) for (λ_1, λ_2) with $\lambda_2 \geq \lambda_{2\max}(\lambda_1)$, which by definition results in the solution $\hat{\beta}(\lambda_1, \infty)$. The problem of finding $\lambda_{2\max}(\lambda_1)$ can be formulated as $\min_{\lambda_2, U, V} \lambda_2$ subject to the optimality conditions (14a)-(14b) where $U = (u_1, \dots, u_T)$ and $V = (v_1, \dots, v_{T-1})$. By eliminating the v_t from (14a), this problem can be formulated as the min-max problem

$$\min_U \max_{1 \leq t \leq T} \frac{1}{w_t} \left\| \sum_{s=1}^t z_s + \lambda_1 \sum_{s=1}^t u_s \right\|_2 \quad (39)$$

subject to the constraints (14b) and $\sum_{t=1}^T z_s + \lambda_1 \sum_{t=1}^T u_t = 0_p$. We leave this nontrivial problem as a direction for future research.

Screening rules. In lasso and fused lasso regression, there exist powerful screening rules for identifying zero coefficients or fused coefficients in solutions before computing these solutions Tibshirani et al. (2012); Wang et al. (2015a,b). Such screening rules often greatly reduce the number of variables to optimize in the objective function and considerably speed up calculations. It would be interesting to see if existing rules can be adapted to the more difficult problem of SGFL or if novel screening rules can be devised for it. A difficulty of SGFL is that it does not possess the monotonic inclusion property of lasso and fused lasso. For example, the fact that two successive vectors $\hat{\beta}_t$ and $\hat{\beta}_{t+1}$ are fused in a SGFL solution $\hat{\beta}(\lambda_1, \lambda_2)$ does *not* imply that they stay fused in a solution $\hat{\beta}(\lambda_1, \lambda'_2)$ with $\lambda'_2 \geq \lambda_2$.

A Proof of Theorem 1

Recall the notations of Section 3.2:

$$\begin{aligned} g(\beta_t) &= \lambda_1 \|\beta_t\|_1 + \lambda_2 w_{t-1} \|\beta_t - \hat{\beta}_{t-1}\|_2 + \lambda_2 w_t \|\beta_t - \hat{\beta}_{t+1}\|_2, \\ g_1(\beta_t) &= \lambda_1 \|\beta_t\|_1, \\ g_2(\beta_t) &= \lambda_2 w_{t-1} \|\beta_t - \hat{\beta}_{t-1}\|_2 + \lambda_2 w_t \|\beta_t - \hat{\beta}_{t+1}\|_2 + (L_t/2) \|\beta_t - z_t\|_2^2, \\ \bar{g}(\beta_t) &= g(\beta_t) + (L_t/2) \|\beta_t - z_t\|_2^2 = g_1(\beta_t) + g_2(\beta_t), \\ \gamma_n &= (L_t + (\lambda_2 w_{t-1} / \|\beta_t^n - \hat{\beta}_{t-1}\|_2) + (\lambda_2 w_t / \|\beta_t^n - \hat{\beta}_{t+1}\|_2))^{-1}, \\ \beta_t^* &= \operatorname{argmin} \bar{g} = \operatorname{prox}_{g/L_t}(z_t), \quad r_n = \bar{g}(\beta_t^n) - \bar{g}(\beta_t^*). \end{aligned}$$

In view of Remark 2 framing the iterative soft-thresholding scheme (23)-(24) as a proximal gradient method, we can establish the linear convergence of this scheme to $\operatorname{prox}_{g/L_t}(z_t)$ by

adapting the results of Bredies and Lorenz (2008) to a nonsmooth setting. Essentially, the proof of linear convergence in Bredies and Lorenz (2008) works by first establishing a lower bound on $\bar{g}(\beta_t^n) - \bar{g}(\beta_t^{n-1})$, the decrease in the objective function between successive iterations of the proximal gradient method (Lemma 1). This general result shows in particular that when using sufficiently small step sizes, the proximal gradient is a descent method. After that, under the additional assumptions that g_2 is convex and that $\|\beta_t^n - \beta_t^{n-1}\|_2^2 \leq cr_n$ for some $c > 0$, the lower bound of Lemma 1 is exploited to show the exponential decay of (r_n) and the linear convergence of (β_t^n) (Proposition 2). In a third movement, the lower bound of Lemma 1 is decomposed as a Bregman-like distance term involving g_1 plus a Taylor remainder term involving g_2 . The specific nature of g_1 (ℓ_1 norm) and possible additional regularity conditions on g_2 (typically, strong convexity) are then used to establish the linear convergence result (Theorem 2). For brevity, we refer the reader to Bredies and Lorenz (2008) for the exact statement of these results.

Lemma 1 and Proposition 2 of Bredies and Lorenz (2008) posit, among other things, that the “smooth” part of the objective, g_2 in our notations, is differentiable everywhere and has a Lipschitz-continuous gradient. In the present case, g_2 is not differentiable at $\hat{\beta}_{t-1}$ and $\hat{\beta}_{t+1}$; however it is differentiable everywhere else and its gradient is Lipschitz-continuous in a local sense. The main effort required for us is to show that Lemma 1 still holds if the points of nondifferentiability of g_2 are not on segments joining the iterates $\beta_t^n, n \geq 0$. Put differently, the iterative soft-thresholding scheme should not cross $\hat{\beta}_{t-1}$ and $\hat{\beta}_{t+1}$ on its path. This is where the requirement that $\bar{g}(\beta_t^0) < \min(\bar{g}(\hat{\beta}_{t-1}), \bar{g}(\hat{\beta}_{t+1}))$ in Theorem 1 plays a crucial part. We now proceed to adapt Lemma 1, after which we will establish the premises of Theorem 2 of Bredies and Lorenz (2008).

Adaptation of Lemma 1 of Bredies and Lorenz (2008). The main result we need prove is that

$$\forall n \in \mathbb{N}, \quad \{\hat{\beta}_{t-1}, \hat{\beta}_{t+1}\} \cap \{\alpha\beta_t^n + (1-\alpha)\beta_t^{n+1} : 0 \leq \alpha \leq 1\} = \emptyset. \quad (40)$$

Once this is established, we may follow the proof of Proposition 2 without modification. In particular, we will be in position to state that

$$\|\nabla g_2(\beta_t^n + \alpha(\beta_t^{n+1} - \beta_t^n)) - \nabla g_2(\beta_t^n)\|_2 \leq \alpha \tilde{L}_n \|\beta_t^{n+1} - \beta_t^n\|_2 \quad (41)$$

for all $n \in \mathbb{N}$ and $\alpha \in [0, 1]$, where

$$\tilde{L}_n = L_t + \frac{2\lambda_2 w_{t-1}}{\|\beta_t^n - \hat{\beta}_{t-1}\|_2} + \frac{2\lambda_2 w_t}{\|\beta_t^n - \hat{\beta}_{t+1}\|_2}.$$

Note that the left-hand side in (41) is not well defined if (40) does not hold. Combining the local Lipschitz property (41) with the step size condition $\gamma_n < 2/\tilde{L}_n$, we may go on to

establish the descent property (3.5) of Bredies and Lorenz (2008):

$$\bar{g}(\beta_t^{n+1}) \leq \bar{g}(\beta_t^n) - \delta D_{\gamma_n}(\beta_t^n) \quad (42)$$

where

$$D_{\gamma_n}(\beta_t^n) = g_1(\beta_t^n) - g_1(\beta_t^{n+1}) + \nabla g_2(\beta_t^n)'(\beta_t^n - \beta_t^{n+1}) \quad \text{and} \quad \delta = 1 - \frac{\max_n \gamma_n \tilde{L}_n}{2}.$$

Lemma 1 shows that $D_{\gamma_n}(\beta_t^n) \geq \|\beta_t^n - \beta_t^{n+1}\|_2^2 / \gamma_n \geq 0$. To show the positivity of δ , note that

$$\gamma_n \tilde{L}_n = 2 - L_t \left(L_t + \frac{\lambda_2 w_{t-1}}{\|\beta_t^n - \hat{\beta}_{t-1}\|_2} + \frac{\lambda_2 w_t}{\|\beta_t^n - \hat{\beta}_{t+1}\|_2} \right)^{-1}.$$

Given the descent property of (β_n) for \bar{g} , the assumption $\bar{g}(\beta_t^0) < \min(\bar{g}(\hat{\beta}_{t-1}), \bar{g}(\hat{\beta}_{t+1}))$, and the convexity of the sublevel sets of \bar{g} , it holds that $\|\beta_t^n - \hat{\beta}_{t-1}\|_2 \geq d(\hat{\beta}_{t-1}, \{\beta_t : \bar{g}(\beta_t) \leq \bar{g}(\beta_t^0)\})$ for all $n \in \mathbb{N}$; an analog inequality holds for $\hat{\beta}_{t+1}$. Denoting these positive lower bounds by m_{t-1} and m_{t+1} , we have

$$0 < \frac{1}{2} \left(1 + \frac{\lambda_2 w_{t-1}}{L_t m_{t-1}} + \frac{\lambda_2 w_t}{L_t m_{t+1}} \right)^{-1} \leq \delta \leq \frac{1}{2}. \quad (43)$$

Together, the step size condition $\gamma_n < 2/\tilde{L}_n$, descent property (42), and lower bound (43) finish to establish Lemma 1 and the precondition of Proposition 2 of Bredies and Lorenz (2008).

It remains to prove (40). We will show a weaker form of (42), namely that $\bar{g}(\beta_t^{n+1}) \leq \bar{g}(\beta_t^n)$ for all n . This inequality, combined with the convexity of \bar{g} and the assumption $\bar{g}(\beta_t^0) < \min(\bar{g}(\hat{\beta}_{t-1}), \bar{g}(\hat{\beta}_{t+1}))$, implies that $\hat{\beta}_{t-1}$ and $\hat{\beta}_{t+1}$ cannot be on a segment joining β_t^n and β_t^{n+1} . Otherwise, the convexity of \bar{g} would imply that, say, $\bar{g}(\hat{\beta}_{t-1}) \leq \max(\bar{g}(\beta_t^n), \bar{g}(\beta_t^{n+1})) \leq \bar{g}(\beta_t^n) \leq \dots \leq \bar{g}(\beta_t^0) < \bar{g}(\hat{\beta}_{t-1})$, a contradiction.

To prove the simple descent property, we start with an easy lemma stated without proof.

Lemma 1. *For all $x, y \in \mathbb{R}^p$ such that $y \neq 0_p$,*

$$\|x\|_2 \leq \|y\|_2 + \frac{y'(x - y)}{\|y\|_2} + \frac{\|x - y\|_2^2}{2\|y\|_2}.$$

Applying this lemma to $x = \beta_t - \hat{\beta}_{t\pm 1}$ and $y = \beta_t^n - \hat{\beta}_{t\pm 1}$, we deduce that for all $\beta_t \in$

\mathbb{R}^p ,

$$\|\beta_t - \hat{\beta}_{t-1}\|_2 \leq \|\beta_t^n - \hat{\beta}_{t-1}\|_2 + \frac{(\beta_t - \hat{\beta}_{t-1})'(\beta_t - \beta_t^n)}{\|\beta_t^n - \hat{\beta}_{t-1}\|_2} + \frac{\|\beta_t - \beta_t^n\|_2^2}{2\|\beta_t^n - \hat{\beta}_{t-1}\|_2}, \quad (44)$$

$$\|\beta_t - \hat{\beta}_{t+1}\|_2 \leq \|\beta_t^n - \hat{\beta}_{t+1}\|_2 + \frac{(\beta_t - \hat{\beta}_{t+1})'(\beta_t - \beta_t^n)}{\|\beta_t^n - \hat{\beta}_{t+1}\|_2} + \frac{\|\beta_t - \beta_t^n\|_2^2}{2\|\beta_t^n - \hat{\beta}_{t+1}\|_2}. \quad (45)$$

In addition, it is immediate that

$$\|\beta_t - z_t\|_2^2 = \|\beta_t^n - z_t\|_2^2 - 2(\beta_t^n - z_t)'(\beta_t - \beta_t^n) + \|\beta_t - \beta_t^n\|_2^2. \quad (46)$$

Multiplying (44) by $\lambda_2 w_{t-1}$, (45) by $\lambda_2 w_t$, (46) by $L_t/2$, summing these relations, and adding $g_1(\beta_t)$ on each side, we obtain

$$(g_1 + g_2)(\beta_t) \leq g_1(\beta_t) + g_2(\beta_t^n) + \nabla g_2(\beta_t^n)'(\beta_t - \beta_t^n) + \frac{1}{2\gamma_n} \|\beta_t - \beta_t^n\|_2^2. \quad (47)$$

The left-hand side of (47) is simply $\bar{g}(\beta_t)$. Also, in view of Remark 2, the minimizer of the right-hand side of (47) is $\mathcal{T}(\beta_t^n) = \beta_t^{n+1}$. Evaluating (47) at β_t^{n+1} and exploiting this minimizing property, it follows that

$$\begin{aligned} \bar{g}(\beta_t^{n+1}) &\leq g_1(\beta_t^{n+1}) + g_2(\beta_t^n) + \nabla g_2(\beta_t^n)'(\beta_t^{n+1} - \beta_t^n) + \frac{1}{2\gamma_n} \|\beta_t^{n+1} - \beta_t^n\|_2^2 \\ &\leq g_1(\beta_t^n) + g_2(\beta_t^n) + \nabla g_2(\beta_t^n)'(\beta_t^{n+1} - \beta_t^n) + \frac{1}{2\gamma_n} \|\beta_t^{n+1} - \beta_t^n\|_2^2 \\ &= \bar{g}(\beta_t^n). \end{aligned} \quad (48)$$

This establishes the desired descent property.

Prerequisites of Theorem 2 of Bredies and Lorenz (2008). The distance $r_n = \bar{g}(\beta_t^n) - \bar{g}(\beta_t^*)$ to the minimum of the objective can be usefully decomposed as

$$\begin{aligned} r_n &= R(\beta_t^n) + T(\beta_t^n) \\ R(\beta_t) &= \nabla g_2(\beta_t^*)'(\beta_t - \beta_t^*) + g_1(\beta_t) - g_1(\beta_t^*) \\ T(\beta_t) &= g_2(\beta_t) - g_2(\beta_t^*) - \nabla g_2(\beta_t^*)'(\beta_t - \beta_t^*) \end{aligned} \quad (49)$$

where $R(\beta_t)$ is a Bregman-like distance and $T(\beta_t)$ is the remainder of the Taylor expansion of g_2 at β_t^* .

To obtain the linear convergence of (β_t^n) to β_t^* and the exponential decay of (r_n) to 0 with Theorem 2 of Bredies and Lorenz (2008), it suffices to show that

$$\|\beta_t - \beta_t^*\|_2^2 \leq c(R(\beta_t) + T(\beta_t)) \quad (50)$$

for some constant $c > 0$ and for all $\beta_t \in \mathbb{R}^p$.

Invoking the convexity of $\|\cdot\|_2$ and strong convexity of $\|\cdot\|_2^2$, one sees that $T(\beta_t) \geq (L_t/2)\|\beta_t - \beta_t^*\|_2^2$ for all β_t . Also, $R(\beta_t) \geq 0$ for all β_t (Lemma 2 of Bredies and Lorenz (2008)) so that c can be taken as $2/L_t$ in (50). \square

B Proof of Theorem 2

We first observe that by design, each of the four steps or components of Algorithm 5 is nonincreasing in the objective function F . Indeed the first three steps (optimization with respect to single blocks, single chains, and descent over fixed chains) are all based on FISTA (Algorithms 3 and 4) which is globally convergent ((Beck and Teboulle, 2009, Theorem 4.4)). As each of these components minimizes F under certain constraints (namely, some blocks or fusion chains are fixed), the objective value of their output, say $F(\beta^{n+1})$, cannot be lower than that of their input, $F(\beta^n)$. The fourth step, subgradient descent is also nonincreasing because the subgradient of minimum norm - if it is not zero - provides a direction of (steepest) descent. The line search for the step size in the subgradient step then guarantees that the objective does not decrease after this step. As a result, Algorithm 5 as a whole is nonincreasing in F .

Let us denote a generic segmentation of the set $\{1, \dots, T\}$ by $C = (C_1, \dots, C_K)$ where $C_k = \{T_k, \dots, T_{k+1} - 1\}$ and $1 = T_1 \leq \dots \leq T_K < T_{K+1} = T + 1$. There are 2^{T-1} such segmentations. Let S_C be the associated open set for the parameter β :

$$S_C = \{\beta \in \mathbb{R}^{pT} : \beta_{T_k} = \dots = \beta_{T_{k+1}-1}, \beta_{T_{k+1}-1} \neq \beta_{T_{k+1}}, 1 \leq k \leq K\}.$$

To each segmentation C is associated an infimum value of F : $\inf_{\beta \in S_C} F(\beta)$. Let $(\beta^n)_{n \geq 0}$ be the sequence of iterates generated by Algorithm 5 and let C^n the associated segmentations of $\{1, \dots, T\}$. By setting the tolerance ϵ of Algorithm 5 sufficiently small, each time the third optimization component (descent over fixed chains) is applied, say with β^n as input and β^{n+1} as output, the objective $F(\beta)$ can be made arbitrarily close to $\min_{\beta \in S_{C^n}} F(\beta)$ or even become inferior to this value if a fusion of chains occurs during this optimization. If the segmentation C^n is optimal, i.e. $\min_{S_{C^n}} F(\beta) = \min_{\beta \in \mathbb{R}^{pT}} F(\beta)$, then Algorithm 5 has converged: for all subsequent iterates $m \geq n$, $F(\beta^m)$ and β^m will stay arbitrarily close to the minimum of F and to the set of minimizers, respectively, because of the nonincreasing property of Algorithm 5. If the segmentation C^n is suboptimal, i.e. $\min_{\beta \in S_{C^n}} F(\beta) > \min_{\beta \in \mathbb{R}^{pT}} F(\beta)$, provided that ϵ is sufficiently small, the (fourth) subgradient step of Algorithm 5 will eventually produce an iterate β^m ($m \geq n$) such that $F(\beta^m) < \min_{\beta \in S_{C^n}} F(\beta)$. This is because each subgradient step brings the iterates closer to the set of global minimizers of F . Once this has happened, the nonincreasing property of the algorithm guarantees that the segmentation C^n will not be visited again. Because the segmentations of $\{1, \dots, T\}$ are in finite number, Algorithm 5 eventually finds an optimal

segmentation C such that $\min_{\beta \in S_C} F(\beta) = \min_{\beta \in \mathbb{R}^{pT}} F(\beta)$. Then, through its third level of optimization (descent over fixed chains), it reaches the global minimum of F . We note that the first and second components of Algorithm 5 (block coordinate descent over single blocks and single chains) are not necessary to ensure global convergence; they only serve for computational speed. \square

References

- Alaíz, C. M., Jiménez, Á. B., and Dorronsoro, J. R. (2013). Group fused lasso. In *Artificial Neural Networks and Machine Learning - ICANN 2013*, pages 66–73.
- Alewijnse, S. P. A., Buchin, K., Buchin, M., Sijben, S., and Westenberg, M. A. (2018). Model-based segmentation and classification of trajectories. *Algorithmica*, 80(8):2422–2452.
- Bai, J. (1997). Estimating multiple breaks one at a time. *Econometric Theory*, 13(3):315–352.
- Bai, J. and Perron, P. (2003). Computation and analysis of multiple structural change models. *Journal of Applied Econometrics*, 18(1):1–22.
- Barbero, A. and Sra, S. (2011). Fast newton-type methods for total variation regularization. In *Proceedings of the 28th International Conference on Machine Learning, ICML 2011*, pages 313–320.
- Basseville, M. and Nikiforov, I. V. (1993). *Detection of abrupt changes: theory and application*. Prentice Hall Information and System Sciences Series. Prentice Hall, Inc., Englewood Cliffs, NJ.
- Beck, A. and Teboulle, M. (2009). A fast iterative shrinkage-thresholding algorithm for linear inverse problems. *SIAM J. Imaging Sci.*, 2(1):183–202.
- Becker, S., Bobin, J., and Candès, E. J. (2011). NESTA: a fast and accurate first-order method for sparse recovery. *SIAM J. Imaging Sci.*, 4(1):1–39.
- Beer, J. C., Aizenstein, H. J., Anderson, S. J., and Krafty, R. T. (2019). Incorporating prior information with fused sparse group lasso: Application to prediction of clinical measures from neuroimages. *Biometrics*, 75(4):1299–1309.
- Bertsekas, D. P. (2015). *Convex optimization algorithms*. Athena Scientific, Belmont, MA.
- Bleakley, K. and Vert, J.-P. (2011). The group fused lasso for multiple change-point detection. Technical Report hal-00602121.
- Boyd, S., Parikh, N., Chu, E., Peleato, B., and Eckstein, J. (2011). Distributed optimization and statistical learning via the Alternating Direction Method of Multipliers. *Found. Trends Mach. Learn.*, 3(1):1–122.
- Bredies, K. and Lorenz, D. A. (2008). Linear convergence of iterative soft-thresholding. *J. Fourier Anal. Appl.*, 14(5-6):813–837.
- Cao, P., Liu, X., Liu, H., Yang, J., Zhao, D., Huang, M., and Zaiane, O. (2018). Generalized fused group lasso regularized multi-task feature learning for predicting cognitive outcomes in Alzheimers disease. *Comput. Methods Programs Biomed.*, 162:19–45.

- Chen, J. and Chen, Z. (2008). Extended Bayesian information criteria for model selection with large model spaces. *Biometrika*, 95(3):759–771.
- Chen, X., Lin, Q., Kim, S., Carbonell, J. G., and Xing, E. P. (2012). Smoothing proximal gradient method for general structured sparse regression. *Ann. Appl. Stat.*, 6(2):719–752.
- Chi, E. C. and Lange, K. (2015). Splitting methods for convex clustering. *J. Comput. Graph. Statist.*, 24(4):994–1013.
- Combettes, P. L. and Pesquet, J.-C. (2011). *Fixed-Point Algorithms for Inverse Problems in Science and Engineering*, chapter Proximal Splitting Methods in Signal Processing, pages 185–212. Springer New York, New York, NY.
- Condat, L. (2013). A primal-dual splitting method for convex optimization involving Lipschitzian, proximable and linear composite terms. *J. Optim. Theory Appl.*, 158(2):460–479.
- De Vito, S., Massera, E., Piga, M., Martinotto, L., and Di Francia, G. (2008). On field calibration of an electronic nose for benzene estimation in an urban pollution monitoring scenario. *Sensors and Actuators B: Chemical*, 129(2):750 – 757.
- De Vito, S., Piga, M., Martinotto, L., and Di Francia, G. (2009). Co, no2 and nox urban pollution monitoring with on-field calibrated electronic nose by automatic bayesian regularization. *Sensors and Actuators B: Chemical*, 143(1):182 – 191.
- Friedman, J., Hastie, T., Höfling, H., and Tibshirani, R. (2007). Pathwise coordinate optimization. *Ann. Appl. Stat.*, 1(2):302–332.
- Fryzlewicz, P. (2014). Wild binary segmentation for multiple change-point detection. *Annals of Statistics*, 42(6):2243.
- Hadj-Salem, F., Löfstedt, T., Dohmatob, E., Frouin, V., Dubois, M., Guillemot, V., and Duchesnay, E. (2018). Continuation of nesterov’s smoothing for regression with structured sparsity in high-dimensional neuroimaging. *IEEE Trans. Medical Imaging*, 37(11):2403–2413.
- Hallac, D., Nystrup, P., and Boyd, S. (2019). Greedy Gaussian segmentation of multivariate time series. *Adv. Data Anal. Classif.*, 13(3):727–751.
- Hocking, T., Vert, J.-P., Bach, F. R., and Joulin, A. (2011). Clusterpath: an algorithm for clustering using convex fusion penalties. In *ICML*.
- Hoefling, H. (2010). A path algorithm for the fused lasso signal approximator. *Journal of Computational and Graphical Statistics*, 19(4):984–1006.
- Kim, S. and Xing, E. P. (2012). Tree-guided group lasso for multi-response regression with

- structured sparsity, with an application to eQTL mapping. *Ann. Appl. Stat.*, 6(3):1095–1117.
- Kuhn, H. W. (1973). A note on Fermat’s problem. *Math. Programming*, 4:98–107.
- Leonardi, F. and Bühlmann, P. (2016). Computationally efficient change point detection for high-dimensional regression.
- Li, X., Mo, L., Yuan, X., and Zhang, J. (2014). Linearized alternating direction method of multipliers for sparse group and fused LASSO models. *Comput. Statist. Data Anal.*, 79:203–221.
- Li, Y. and Osher, S. (2009). Coordinate descent optimization for ℓ^1 minimization with application to compressed sensing; a greedy algorithm. *Inverse Probl. Imaging*, 3(3):487–503.
- Liu, J., Yuan, L., and Ye, J. (2010). An efficient algorithm for a class of fused lasso problems. In *Proceedings of the 16th ACM SIGKDD international conference on knowledge discovery and data mining*, KDD ’10, pages 323–332. ACM.
- Nesterov, Y. (2005). Smooth minimization of non-smooth functions. *Math. Program.*, 103(1, Ser. A):127–152.
- Nesterov, Y. (2012). Efficiency of coordinate descent methods on huge-scale optimization problems. *SIAM J. Optim.*, 22(2):341–362.
- Nystrup, P., Madsen, H., and Lindström, E. (2017). Long memory of financial time series and hidden Markov models with time-varying parameters. *J. Forecast.*, 36(8):989–1002.
- Ohlsson, H., Ljung, L., and Boyd, S. (2010). Segmentation of ARX-models using sum-of-norms regularization. *Automatica*, 46(6):1107–1111.
- Ombao, H., von Sachs, R., and Guo, W. (2005). Slex analysis of multivariate nonstationary time series. *J. Amer. Statist. Assoc.*, 100(470):519–531.
- Price, B. S., Geyer, C. J., and Rothman, A. J. (2019). Automatic response category combination in multinomial logistic regression. *J. Comput. Graph. Statist.*, 28(3):758–766.
- R Core Team (2019). *R: A Language and Environment for Statistical Computing*. R Foundation for Statistical Computing, Vienna, Austria.
- Ranalli, M., Lagona, F., Picone, M., and Zambianchi, E. (2018). Segmentation of sea current fields by cylindrical hidden markov models: a composite likelihood approach. *Journal of the Royal Statistical Society: Series C (Applied Statistics)*, 67(3):575–598.
- Rockafellar, R. (2015). *Convex Analysis*. Princeton Landmarks in Mathematics and Physics. Princeton University Press.

- Sanderson, C. and Curtin, R. (2016). Armadillo: a template-based C++ library for linear algebra. *Journal of Open Source Software*, 1:26.
- Saxén, J.-E., Saxén, H., and Toivonen, H. T. (2016). Identification of switching linear systems using self-organizing models with application to silicon prediction in hot metal. *Applied Soft Computing*, 47:271 – 280.
- Shor, N. Z. (1985). *Minimization methods for nondifferentiable functions*, volume 3 of *Springer Series in Computational Mathematics*. Springer-Verlag, Berlin. Translated from the Russian by K. C. Kiwiel and A. Ruszczyński.
- Songsiri, J. (2015). Learning multiple granger graphical models via group fused lasso. In *2015 10th Asian Control Conference (ASCC)*, pages 1–6.
- Tibshirani, R., Bien, J., Friedman, J., Hastie, T., Simon, N., Taylor, J., and Tibshirani, R. J. (2012). Strong rules for discarding predictors in lasso-type problems. *J. R. Stat. Soc. Ser. B. Stat. Methodol.*, 74(2):245–266.
- Tibshirani, R. and Wang, P. (2007). Spatial smoothing and hot spot detection for CGH data using the fused lasso. *Biostatistics*, 9(1):18–29.
- Truong, C., Oudre, L., and Vayatis, N. (2018). A review of change point detection methods. *CoRR*, abs/1801.00718.
- Tseng, P. (2001). Convergence of a block coordinate descent method for nondifferentiable minimization. *J. Optim. Theory Appl.*, 109(3):475–494.
- Vũ, B. C. (2013). A variable metric extension of the forward-backward-forward algorithm for monotone operators. *Numer. Funct. Anal. Optim.*, 34(9):1050–1065.
- Wang, B., Zhang, Y., Sun, W. W., and Fang, Y. (2018). Sparse convex clustering. *J. Comput. Graph. Statist.*, 27(2):393–403.
- Wang, J., Fan, W., and Ye, J. (2015a). Fused lasso screening rules via the monotonicity of subdifferentials. *IEEE Transactions on Pattern Analysis and Machine Intelligence*, 37(9):1806–1820.
- Wang, J., Wonka, P., and Ye, J. (2015b). Lasso screening rules via dual polytope projection. *J. Mach. Learn. Res.*, 16:1063–1101.
- Wang, T. and Zhu, L. (2011). Consistent tuning parameter selection in high dimensional sparse linear regression. *J. Multivariate Anal.*, 102(7):1141–1151.
- Weiszfeld, E. and Plastria, F. (2009). On the point for which the sum of the distances to n given points is minimum. *Annals of Operations Research*, 167(1):7–41.
- Wytock, M., Sra, S., and Kolter, J. Z. (2014). Fast Newton methods for the group fused lasso. In *Uncertainty in Artificial Intelligence, UAI 2014*, pages 888–897.

- Xu, Y. and Lindquist, M. (2015). Dynamic connectivity detection: an algorithm for determining functional connectivity change points in fMRI data. *Frontiers in Neuroscience*, 9:285.
- Yan, M. (2018). A new primal–dual algorithm for minimizing the sum of three functions with a linear operator. *J. Sci. Comput.*, 76(3):1698–1717.
- Yao, Y.-C. (1988). Estimating the number of change-points via Schwarz’ criterion. *Statist. Probab. Lett.*, 6(3):181–189.
- Yuan, M. and Lin, Y. (2006). Model selection and estimation in regression with grouped variables. *J. R. Stat. Soc. Ser. B Stat. Methodol.*, 68(1):49–67.
- Zhou, J., Liu, J., Narayan, V. A., and Ye, J. (2013). Modeling disease progression via multi-task learning. *NeuroImage*, 78:233–248.
- Zhu, C., Xu, H., Leng, C., and Yan, S. (2014). Convex optimization procedure for clustering: Theoretical revisit. In *NIPS*.
- Zou, H. and Hastie, T. (2005). Regularization and variable selection via the elastic net. *J. R. Stat. Soc. Ser. B Stat. Methodol.*, 67(2):301–320.

Supplementary Materials for “Sparse Group Fused Lasso for Model Segmentation”

This document contains additional simulation results in complement of section 4.2 (Simulations: statistical accuracy) of the main manuscript. These results were obtained in the same simulation setup as section 4.2 but with different values of the simulation parameters s (sparsity level of regression vectors), ρ_X (correlation level among predictors), and/or σ_ε (noise level).

Statistical accuracy

This section provides additional results on statistical accuracy. As in section 4.2, the following tables have columns that indicate the estimation method, selection method for regularization parameters, number of change points, Hausdorff distance between estimated and true change points, true positive rate and positive predictive value in detecting nonzero regression coefficients, sparsity level, and pseudo- R^2 . Results are averaged over all replications of a setup, with standard deviations in brackets. The best results for the HBIC selection method are in bold.

Table 5 shows results under the following scenario: sparsity level $s = 0.99$, model dimensions $(d, p, T) = (20, 200, 100)$ or $(d, p, T) = (100, 500, 200)$, no correlation between predictors ($\rho_X = 0$). In comparison to Table 3 of the main article, the noise levels $\sigma_\varepsilon = 0$ (no noise) and $\sigma_\varepsilon = 2.5$ (high noise) are examined. The excellent performances of the BSA and 2S methods in a noiseless situation are confirmed as well as their breakdown in high noise. Also confirmed is the lesser performance of SGFL in recovering nonzero coefficients in low noise ($\sigma_\varepsilon = 0$) and its super performance in high noise ($\sigma_\varepsilon = 2.5$). The high-dimensional setup does not seem to affect statistical performance although, as noted in the main article, the increase in d (20 to 100) and p (100 to 500) may be counterbalanced by the increase in T (100 to 200), which makes the model segments longer and the associated change points (possibly) easier to detect.

Table 5: Simulation study of statistical accuracy. True sparsity level $s = 0.99$, correlation $\rho_X = 0$, number of replications: 100.

Setup	Method	λ	NCP	d_H	TPR	PPV	\hat{s}	R^2
$d = 20$ $p = 200$ $T = 100$ $\sigma_\varepsilon = 0$ {21, 51, 91}	BSA	HBIC	3.0 (0.0)	0.0 (0.0)	1.00 (0.00)	1.00 (0.00)	0.99 (0.00)	1.00 (0.00)
	2S	HBIC	3.4 (0.6)	0.4 (0.5)	1.00 (.02)	1.00 (0.02)	0.99 (0.00)	1.00 (0.00)
	SGFL	HBIC	3.0 (0.1)	1.1 (5.6)	0.93 (.09)	0.72 (0.11)	0.99 (0.00)	0.96 (0.01)
	BSA	d_H	3.0 (0.0)	0.0 (0.0)	1.00 (.01)	1.00 (0.00)	0.99 (0.00)	1.00 (0.00)
	2S	d_H	3.4 (0.5)	0.4 (0.5)	1.00 (.02)	1.00 (0.01)	0.99 (0.00)	0.97 (0.05)
	SGFL	d_H	3.0 (0.0)	0.0 (0.0)	0.91 (.10)	0.93 (0.13)	0.99 (0.02)	0.86 (0.10)
	BSA	HBIC	3.0 (0.0)	0.0 (0.0)	1.00 (0.01)	1.00 (0.00)	0.99 (0.99)	1.00 (0.00)
	2S	HBIC	3.0 (0.0)	0.0 (0.0)	1.00 (0.01)	1.00 (0.00)	0.99 (0.99)	1.00 (0.00)
	SGFL	HBIC	3.0 (0.0)	0.0 (0.0)	0.97 (0.04)	0.51 (0.05)	0.98 (0.00)	0.97 (0.00)
$d = 100$ $p = 500$ $T = 200$ $\sigma_\varepsilon = 0$ {41, 101, 81}	BSA	d_H	3.0 (0.0)	0.0 (0.0)	1.00 (0.01)	1.00 (0.00)	0.99 (0.00)	1.00 (0.00)
	2S	d_H	3.0 (0.0)	0.0 (0.0)	1.00 (0.01)	1.00 (0.00)	0.99 (0.00)	0.99 (0.02)
	SGFL	d_H	3.0 (0.0)	0.0 (0.0)	0.89 (0.06)	0.94 (0.05)	0.99 (0.00)	0.90 (0.06)
	BSA	HBIC	1.6 (1.2)	95.0 (77.1)	0.98 (0.03)	0.02 (0.00)	0.45 (0.10)	0.35 (0.17)
	2S	HBIC	4.4 (1.8)	18.8 (32.2)	0.84 (0.14)	0.82 (0.10)	0.99 (0.00)	0.40 (0.10)
	SGFL	HBIC	3.0 (0.2)	2.3 (12.7)	0.81 (0.12)	0.95 (0.05)	0.99 (0.00)	0.37 (0.09)
$d = 100$ $p = 500$ $T = 200$ $\sigma_\varepsilon = 2.5$ {41, 101, 181}	BSA	d_H	3.0 (0.0)	0.0 (0.0)	0.99 (0.02)	1.00 (0.02)	0.99 (0.00)	0.99 (0.00)
	2S	d_H	3.0 (0.2)	0.0 (0.2)	0.98 (0.03)	1.00 (0.01)	0.99 (0.00)	0.98 (0.01)
	SGFL	d_H	3.0 (0.0)	0.0 (0.0)	0.90 (0.08)	0.94 (0.04)	0.99 (0.00)	0.89 (0.05)

Table 6 displays results for the setup $s = 0.90$, $(d, p, T) = (100, 500, 200)$, and $\rho_X = 0$. Only 10 replications were performed in this case due to the large computational demand of the high model dimensions. The table shows a better performance of BSA and 2S, in comparison to the situation where $s = 0.99$. This can be interpreted as follows: the lower sparsity $s = 0.90$ produces more marked changes between regression vectors β_t at the change points $t = T_k$. More precisely, the jump size $\|\beta_{T_{k+1}} - \beta_{T_k}\|$ becomes larger (in expected value). As a result, change points become easier to detect, which improves performance.

Table 6: Simulation study of statistical accuracy. True sparsity level $s = 0.90$, correlation $\rho_X = 0$, number of replications: 10.

Setup	Method	λ	NCP	d_H	TPR	PPV	\hat{s}	R^2
$d = 100$ $p = 500$ $T = 200$ $\sigma_\varepsilon = 0$ {41, 101, 181}	BSA	HBIC	3.0 (0.0)	0.0 (0.0)	1.00 (0.00)	1.00 (0.00)	0.90 (0.00)	1.00 (0.00)
	2S	HBIC	3.0 (0.0)	0.0 (0.0)	1.00 (0.00)	1.00 (0.00)	0.90 (0.00)	1.00 (0.00)
	SGFL	HBIC	3.0 (0.0)	0.0 (0.0)	0.90 (0.03)	0.86 (0.03)	0.90 (0.01)	0.94 (0.01)
	BSA	d_H	3.0 (0.0)	0.0 (0.0)	1.00 (0.00)	1.00 (0.00)	0.90 (0.00)	1.00 (0.00)
	2S	d_H	3.0 (0.0)	0.0 (0.0)	1.00 (0.00)	1.00 (0.00)	0.90 (0.00)	1.00 (0.00)
	SGFL	d_H	3.0 (0.0)	0.0 (0.0)	0.87 (0.03)	0.92 (0.03)	0.91 (0.01)	0.93 (0.01)
$d = 100$ $p = 500$ $T = 200$ $\sigma_\varepsilon = 0.25$ {41, 101, 181}	BSA	HBIC	3.0 (0.0)	0.0 (0.0)	0.99 (0.01)	0.99 (0.01)	0.90 (0.0)	1.00 (0.00)
	2S	HBIC	3.0 (0.0)	0.0 (0.0)	0.99 (0.01)	0.98 (0.01)	0.90 (0.0)	1.00 (0.00)
	SGFL	HBIC	3.0 (0.0)	0.0 (0.0)	0.89 (0.04)	0.89 (0.03)	0.90 (0.01)	0.92 (0.01)
	BSA	d_H	3.0 (0.0)	0.0 (0.0)	0.99 (0.01)	1.00 (0.00)	0.90 (0.00)	1.00 (0.00)
	2S	d_H	3.0 (0.0)	0.0 (0.0)	0.99 (0.01)	1.00 (0.00)	0.90 (0.00)	1.00 (0.00)
	SGFL	d_H	3.0 (0.0)	0.0 (0.0)	0.87 (0.04)	0.93 (0.02)	0.91 (0.00)	0.92 (0.01)
$d = 100$ $p = 500$ $T = 200$ $\sigma_\varepsilon = 1.0$ {41, 101, 181}	BSA	HBIC	3.0 (0.0)	0.0 (0.0)	0.97 (0.01)	0.88 (0.07)	0.89 (0.01)	0.98 (0.00)
	2S	HBIC	3.0 (0.0)	0.0 (0.0)	0.96 (0.01)	0.98 (0.00)	0.90 (0.00)	0.98 (0.00)
	SGFL	HBIC	3.0 (0.0)	0.0 (0.0)	0.89 (0.04)	0.89 (0.03)	0.90 (0.01)	0.92 (0.01)
	BSA	d_H	3.0 (0.0)	0.0 (0.0)	0.97 (0.01)	0.88 (0.07)	0.89 (0.01)	0.98 (0.00)
	2S	d_H	3.0 (0.0)	0.0 (0.0)	0.95 (0.01)	0.99 (0.01)	0.90 (0.00)	0.98 (0.00)
	SGFL	d_H	3.0 (0.0)	0.0 (0.0)	0.88 (0.04)	0.93 (0.02)	0.91 (0.00)	0.90 (0.02)
$d = 100$ $p = 500$ $T = 200$ $\sigma_\varepsilon = 2.5$ {41, 101, 181}	BSA	HBIC	3.0 (0.0)	0.0 (0.0)	0.97 (0.01)	0.28 (0.03)	0.65 (0.04)	0.89 (0.01)
	2S	HBIC	3.0 (0.0)	0.0 (0.0)	0.89 (0.02)	0.97 (0.01)	0.91 (0.00)	0.87 (0.01)
	SGFL	HBIC	3.0 (0.0)	0.0 (0.0)	0.84 (0.03)	0.92 (0.02)	0.91 (0.00)	0.81 (0.01)
	BSA	d_H	3.0 (0.0)	0.0 (0.0)	0.97 (0.01)	0.28 (0.03)	0.65 (0.04)	0.89 (0.01)
	2S	d_H	3.0 (0.0)	0.0 (0.0)	0.90 (0.03)	0.97 (0.01)	0.91 (0.00)	0.87 (0.01)
	SGFL	d_H	3.0 (0.0)	0.0 (0.0)	0.83 (0.02)	0.95 (0.02)	0.91 (0.00)	0.80 (0.02)

Table 7 displays results for the setup $s = 0.90$, $(d, p, T) = (20, 200, 100)$, and $\rho_X = 0$. The results of this table are qualitatively very similar to those of 6. In comparison to Table 3 of the main article, they show that the increase in “signal amplitude” associated to the decrease in sparsity of the regression vectors β_t (from $s = 0.99$ to $s = 0.90$) offsets the increase in noise so that even when $\sigma_\varepsilon = 1.0$ or $\sigma_\varepsilon = 2.5$, the statistical performance of these methods remains good.

Table 7: Simulation study of statistical accuracy. True sparsity level $s = 0.90$, correlation $\rho_X = 0$, number of replications: 100.

Setup	Method	λ	NCP	d_H	TPR	PPV	\hat{s}	R^2
$d = 20$	BSA	HBIC	3.0 (0.0)	0.0 (0.0)	1.00 (0.00)	1.00 (0.00)	0.90 (0.00)	1.00 (0.00)
	2S	HBIC	3.3 (0.5)	0.3 (0.5)	1.00 (0.01)	0.99 (0.01)	0.90 (0.00)	1.00 (0.00)
	SGFL	HBIC	3.0 (0.0)	0.0 (0.0)	0.84 (0.05)	0.85 (0.04)	0.90 (0.01)	0.91 (0.02)
$p = 200$	BSA	d_H	3.0 (0.0)	0.0 (0.0)	1.00 (0.00)	1.00 (0.00)	0.90 (0.00)	1.00 (0.00)
	2S	d_H	3.3 (0.5)	0.3 (0.5)	1.00 (0.01)	0.99 (0.01)	0.90 (0.00)	1.00 (0.00)
	SGFL	d_H	3.0 (0.0)	0.0 (0.0)	0.83 (0.05)	0.89 (0.04)	0.91 (0.01)	0.89 (0.03)
$T = 100$	BSA	HBIC	3.0 (0.0)	0.0 (0.0)	0.96 (0.02)	0.98 (0.01)	0.90 (0.00)	0.99 (0.00)
	2S	HBIC	3.4 (0.5)	0.4 (0.5)	0.95 (0.03)	0.96 (0.01)	0.90 (0.00)	0.99 (0.00)
	SGFL	HBIC	3.0 (0.0)	0.0 (0.0)	0.83 (0.05)	0.84 (0.04)	0.90 (0.01)	0.91 (0.02)
$\sigma_\varepsilon = 0$	BSA	d_H	3.0 (0.0)	0.0 (0.0)	0.96 (0.02)	0.99 (0.01)	0.90 (0.00)	0.99 (0.00)
	2S	d_H	3.4 (0.5)	0.4 (0.5)	0.95 (0.02)	0.98 (0.01)	0.90 (0.00)	0.99 (0.00)
	SGFL	d_H	3.0 (0.0)	0.0 (0.0)	0.81 (0.05)	0.89 (0.05)	0.91 (0.01)	0.89 (0.03)
$\{21, 51, 91\}$	BSA	HBIC	3.0 (0.1)	0.1 (1.0)	0.93 (0.03)	0.61 (0.13)	0.84 (0.04)	0.95 (0.01)
	2S	HBIC	3.5 (0.6)	0.5 (0.5)	0.87 (0.05)	0.91 (0.03)	0.90 (0.01)	0.93 (0.01)
	SGFL	HBIC	3.0 (0.3)	1.1 (10.0)	0.77 (0.11)	0.84 (0.11)	0.91 (0.02)	0.82 (0.11)
$d = 20$	BSA	d_H	3.0 (0.1)	0.1 (1.0)	0.93 (0.03)	0.61 (0.13)	0.84 (0.04)	0.95 (0.01)
	2S	d_H	3.5 (0.6)	0.5 (0.5)	0.87 (0.05)	0.95 (0.03)	0.91 (0.01)	0.92 (0.01)
	SGFL	d_H	3.0 (0.0)	0.0 (0.0)	0.77 (0.06)	0.86 (0.08)	0.91 (0.02)	0.8 (0.06)
$p = 200$	BSA	HBIC	2.7 (0.9)	11.1 (29.4)	0.91 (0.04)	0.21 (0.04)	0.56 (0.10)	0.75 (0.16)
	2S	HBIC	4.1 (1.4)	13.3 (17.5)	0.69 (0.08)	0.82 (0.06)	0.92 (0.01)	0.67 (0.09)
	SGFL	HBIC	2.7 (0.4)	10.7 (17.3)	0.62 (0.12)	0.79 (0.11)	0.92 (0.02)	0.50 (0.12)
$T = 100$	BSA	d_H	3.0 (0.2)	0.5 (2.1)	0.91 (0.03)	0.22 (0.03)	0.58 (0.06)	0.80 (0.03)
	2S	d_H	5.6 (2.0)	3.2 (4.2)	0.71 (0.05)	0.86 (0.07)	0.92 (0.01)	0.69 (0.04)
	SGFL	d_H	3.0 (0.0)	0.0 (0.0)	0.66 (0.08)	0.76 (0.16)	0.90 (0.06)	0.49 (0.09)
$\sigma_\varepsilon = 2.5$	BSA	HBIC	2.7 (0.9)	11.1 (29.4)	0.91 (0.04)	0.21 (0.04)	0.56 (0.10)	0.75 (0.16)
	2S	HBIC	4.1 (1.4)	13.3 (17.5)	0.69 (0.08)	0.82 (0.06)	0.92 (0.01)	0.67 (0.09)
	SGFL	HBIC	2.7 (0.4)	10.7 (17.3)	0.62 (0.12)	0.79 (0.11)	0.92 (0.02)	0.50 (0.12)
$\{21, 51, 91\}$	BSA	d_H	3.0 (0.2)	0.5 (2.1)	0.91 (0.03)	0.22 (0.03)	0.58 (0.06)	0.80 (0.03)
	2S	d_H	5.6 (2.0)	3.2 (4.2)	0.71 (0.05)	0.86 (0.07)	0.92 (0.01)	0.69 (0.04)
	SGFL	d_H	3.0 (0.0)	0.0 (0.0)	0.66 (0.08)	0.76 (0.16)	0.90 (0.06)	0.49 (0.09)

Finally, Table 8 shows results in the setup $s = 0.99$, $(d, p, T) = (20, 200, 100)$, and $\rho_X = 0.5$. There, the presence of relatively strong correlation among predictors has little to no effect on the performance of the BSA method (compare to Table 5 and Table 3 of the main article where $\rho_X = 0$). The correlation slightly degrades the performance of the 2S method and more substantially degrades that of the SGFL, at least when the HBIC is used to select regularization parameters. On the other hand, the fact that the best HBIC parameter for SGFL is $\gamma = 1$ (at the boundary of the γ range) suggest an overpenalization of model complexity. Indeed, the lines SGFL/ d_H show that at least for some choice of (λ_1, λ_2) , the SGFL performance can be satisfactory and on par with the other two methods.

Table 8: Simulation study of statistical accuracy. True sparsity level $s = 0.99$, correlation $\rho_X = 0.5$, number of replications: 100.

Setup	Method	λ	NCP	d_H	TPR	PPV	\hat{s}	R^2
$d = 20$ $p = 200$ $T = 100$ $\sigma_\varepsilon = 0$ {21, 51, 91}	BSA	HBIC	3.0 (0.2)	0.3 (1.8)	1.00 (0.01)	0.99 (0.09)	0.99 (0.01)	1.00 (0.00)
	2S	HBIC	4.3 (1.8)	5.6 (11.1)	0.99 (0.04)	0.95 (0.11)	0.99 (0.00)	0.99 (0.03)
	SGFL	HBIC	2.3 (1.2)	24.2 (38.7)	0.85 (0.19)	0.28 (0.15)	0.95 (0.06)	0.73 (0.31)
	BSA	d_H	3.0 (0.0)	0.0 (0.0)	1.00 (0.01)	1.00 (0.00)	0.99 (0.00)	1.00 (0.00)
	2S	d_H	4.3 (1.7)	5.2 (10.9)	0.98 (0.06)	0.97 (0.06)	0.99 (0.00)	0.96 (0.10)
	SGFL	d_H	3.1 (0.7)	2.0 (7.3)	0.89 (0.14)	0.55 (0.43)	0.79 (0.32)	0.69 (0.24)
$d = 20$ $p = 200$ $T = 100$ $\sigma_\varepsilon = 0.25$ {21, 51, 91}	BSA	HBIC	3.0 (0.4)	1.8 (10.3)	0.96 (0.07)	0.52 (0.31)	0.96 (0.06)	0.94 (0.05)
	2S	HBIC	4.7 (2.1)	8.3 (12.2)	0.90 (0.12)	0.85 (0.15)	0.99 (0.00)	0.92 (0.06)
	SGFL	HBIC	2.0 (1.3)	32.5 (41.3)	0.80 (0.22)	0.38 (0.22)	0.96 (0.06)	0.62 (0.32)
	BSA	d_H	3.0 (0.2)	0.4 (2.0)	0.97 (0.07)	0.52 (0.31)	0.96 (0.04)	0.94 (0.03)
	2S	d_H	5.1 (2.3)	6.2 (10.0)	0.91 (0.10)	0.94 (0.08)	0.99 (0.00)	0.87 (0.10)
	SGFL	d_H	3.4 (1.3)	2.2 (6.0)	0.91 (0.13)	0.47 (0.45)	0.73 (0.35)	0.62 (0.22)

Computation time

Table 9 displays the average runtime per replication for each method (BSA, 2S, SGFL) in each simulation setup. Clearly, 2S is the fastest method of the three by at least 1 order of magnitude. SGFL is the second fastest and BSA last. On average, 2S is about 40 times as fast as SGFL, which in turn is 2 times as fast as BSA.

One information not shown in the table is the size of the grid at which the methods were evaluated. The grid size largely affects the runtime of the BSA and SGFL methods but almost not that of 2S. Indeed, the first step of 2S, group lasso, can be implemented quickly for any single regularization parameter λ_2 and warm starts can be exploited along the regularization path to speed up calculations. The second step of 2S, standard lasso, can calculate fits $\hat{\beta} = \hat{\beta}(\lambda_1)$ for any number of regularization parameters λ_1 essentially for free thanks to its pathwise properties. In contrast, every model fit has a nontrivial cost for BSA and SGFL. For BSA, it appears infeasible to efficiently implement pathwise lasso regression because the segments produced by the binary search are in general different for each λ (one cannot keep track of a segmentation for each λ). For SGFL, warm start methods do not

Table 9: Average computation time per simulation replicate (in seconds, standard deviations in brackets).

d	p	T	s	σ	ρ_X	NCP	BSA	2S	SGFL
20	200	100	0.99	0.25	0.00	3	515 (69)	16 (2)	290 (53)
20	200	100	0.99	1.00	0.00	3	564 (76)	19 (3)	353 (63)
20	200	100	0.99	0.00	0.00	4	486 (57)	15 (2)	316 (56)
20	200	100	0.99	0.25	0.00	4	500 (61)	16 (3)	334 (64)
20	200	100	0.99	1.00	0.00	4	546 (62)	19 (3)	370 (78)
100	500	200	0.99	0.00	0.00	3	20941 (3454)	114 (19)	8341 (1294)
100	500	200	0.99	0.25	0.00	3	20778 (3270)	116 (22)	8331 (1204)
100	500	200	0.99	1.00	0.00	3	20997 (3670)	135 (28)	8242 (1307)
100	500	200	0.99	2.50	0.00	3	21926 (3820)	217 (42)	9472 (1485)
100	500	200	0.90	0.00	0.00	3	18597 (36)	100 (4)	7841 (227)
100	500	200	0.90	0.25	0.00	3	18593 (41)	98 (6)	7901 (232)
100	500	200	0.90	1.00	0.00	3	18746 (105)	100 (9)	7848 (277)
100	500	200	0.90	2.50	0.00	3	19509 (165)	114 (5)	8308 (159)
20	200	100	0.90	0.00	0.00	3	620 (58)	14 (2)	354 (60)
20	200	100	0.90	0.25	0.00	3	635 (56)	14 (2)	360 (58)
20	200	100	0.90	1.00	0.00	3	671 (59)	15 (2)	393 (61)
20	200	100	0.90	2.50	0.00	3	727 (64)	18 (3)	518 (83)
20	200	100	0.99	0	0.50	3	2690 (2155)	15 (5)	833 (1292)
20	200	100	0.99	0.25	0.50	3	3202 (2988)	15 (6)	1046 (1694)

reduce by much the computational cost of a grid evaluation.

Importantly, BSA and SGFL take an excessively long time to compute when the regularization parameter λ or (λ_1, λ_2) is taken too small (this typically lead to a lengthy search for optimal segmentation and a final result with far too many segments/change points). One way to avoid this behavior is through pilot attempts, making sure that the smallest value in a regularization grid is not too small. A related approach is through the use of stopping rules: stop the pathwise regularization whenever the number of segments or nonzero regression coefficients exceeds a threshold. A third way to avoid spending excessive time fitting the model for small λ is to limit the maximum number of iterations of each method. We have used some of these techniques in our simulations to keep the computation time manageable although no attempt at optimizing the computation time was made.

We finally note that in practice, when implementing any of the three above pathwise regularization methods, computations can be efficiently parallelized, which may well reduce the computation time to a fraction of the values reported in Table 9.